

# Sidebands shifts and induced sidebands in rf-dressed Rydberg systems

M. Tanasittikosol\* and R. M. Potvliege†

*Joint Quantum Centre (JQC) Durham-Newcastle,  
Department of Physics, Durham University,  
South Road, Durham DH1 3LE, UK*

## Abstract

The effect of an ac modulation on a 2-level or 3-level system is studied theoretically. The absorption spectrum is calculated by solving the optical Bloch equations and is interpreted by reference to the Floquet quasienergy spectrum. The dependence of the absorption sidebands on the intensity of the coupling laser field in Rydberg systems submitted to a radio-frequency (rf) field is analysed in detail. It is shown that for sufficiently strong coupling fields additional sidebands appear in the probe absorption spectrum in ladder 3-level systems. These additional sidebands are induced by the coupling of the intermediate state to the Floquet manifold spawned by the upper state under rf modulation.

PACS numbers: 32.80.Rm,32.80.Ee,42.50.Gy

---

\*Present address: Theoretical and Computational Physics (TCP) Group, Department of Physics, King Mongkut's University of Technology Thonburi, Bangkok 10140, Thailand.

†Electronic address: r.m.potvliege@durham.ac.uk

## I. INTRODUCTION

There is currently much interest for electromagnetically induced transparency (EIT) in Rydberg atoms [1], in particular for the cooperative atom-light and photon-photon dynamics found in Rydberg systems [2–5] and for their possible application, e.g., in quantum information processing [6], in the production of correlated photon pairs [7], and in metrology [8, 9]. The present work is motivated by a recent experimental study of EIT in a 3-level Rydberg system with radio frequency (rf) modulation [10]. In this experiment, the absorption on the  $5S_{1/2}$ – $5P_{3/2}$  transition of  $^{87}\text{Rb}$  was probed by a weak laser field in the presence of both an rf field and a strong laser field resonant with the transition between the intermediate  $5P_{3/2}(F' = 3)$  state and the highly polarizable  $32S_{1/2}(F' = 2)$  state. The rf field was too low in frequency for driving multiphoton transitions between the lower, intermediate or upper states and other bound states. However, it was strong enough to Stark-shift the upper state periodically by tens of MHz, which resulted into the EIT features in the probe absorption spectrum shifting and splitting into multiple EIT sidebands.

The existence of absorption sidebands is a well known feature of ac-modulated 2-level systems [11], including 2-level atomic or molecular systems [12–19]. The effect of an oscillating electric field on molecular absorption lines with quadratic Stark shift was described by Townes and Merritt in 1947 [13]: Lines whose frequency width is much larger than the frequency of modulation adiabatically follow the oscillations of the field — i.e., a state of dipole polarizability  $\alpha$  in a non-resonant ac field  $\mathcal{E}(t) = \mathcal{E}_0 \sin(\omega_0 t)$  is simply displaced in energy by  $\alpha[\mathcal{E}(t)]^2/2$  at time  $t$ . However, lines whose frequency width is of the same order or smaller than the modulation frequency split into manifolds of components displaced in energy from their zero-field limit by  $\alpha\mathcal{E}_0^2/4 + 2n\hbar\omega_0$ ,  $n = 0, \pm 1, \pm 2, \dots$ , and the intensity of these components varies with  $n$ ,  $\omega_0$  and  $\mathcal{E}_0$  like  $J_n^2(\alpha\mathcal{E}_0/8\hbar\omega_0)$ . Analogous shifts and sidebands are also found in systems governed by an Hamiltonian unitarily equivalent to that governing ac-modulated 2-level atomic or molecular systems, such as ac-driven superconducting flux qubits [20–27].

Interactions with other fields will in general introduce additional  $n$ -dependent Stark shifts. For this reason, the separation between adjacent sidebands of an ac modulated 2-level system is not exactly  $2\hbar\omega_0$  and the intensities of the absorption lines do not exactly follow a  $J_n^2(\alpha\mathcal{E}_0/8\hbar\omega_0)$  law. The correct separations and scalings can be obtained by combining

Floquet theory and Van Vleck perturbation theory [25, 27]. However, these deviations from the results of Townes and Merritt are significant only when the interaction coupling the two states of the system is sufficiently strong. Perhaps for this reason, they do not appear to have been previously considered in an atomic and molecular physics context [28].

In many ac-modulated 2-level atomic systems of practical interest, one of the two states is much more polarizable than the other and the frequency widths of both the state and the coupling laser field are small compared to the modulation frequency. In these conditions, it may be tempting to ignore the manifold structure of the less polarizable state, retain that of the more polarizable state, and model the ac-modulated two-level system as a many-level system in which the less polarizable state interacts with a manifold of independent sideband states. We refer to this approximate description as the  $N$ -level approximation. It leads to the results described by Townes and Merritt [13] in the limit of a weak interaction between the states and makes it possible to calculate the absorption spectrum rapidly at a minimal cost. However, as is shown below, this approximation breaks down for strong coupling between the two states: In order to obtain the correct results, the sideband structure of both states must be properly taken into account. This can be done, e.g., by carrying out a full Floquet analysis of the ac-modulated 2-level system [25, 27, 29–32], or by solving the optical Bloch equations with time-dependent modulation. The sidebands of the less polarizable state here originate from the coupling of this state to the Floquet manifold formed by the other state, not from a direct effect of the ac-modulation. Nonetheless, as is illustrated below, they may manifest by well defined, additional resonance structures in absorption spectra. We refer to these as induced sidebands.

In this paper, we investigate the changes in the sideband structure of the absorption spectrum arising from the interaction with the coupling laser field, both in two-level and three-level systems. The absorption spectrum is calculated by solving the optical Bloch equations and is interpreted by reference to the Floquet quasienergy spectrum. The  $N$ -level approximation is compared to the exact results throughout the paper. For simplicity, we first focus on ac-modulated two-level systems (Sec. II). The coupling with a lower state is then introduced. The probe absorption in an rf-modulated 3-state ladder system and the appearance of induced sidebands is studied in Sec. III. In particular, we give examples of sidebands shift in EIT spectra for both cold and thermal ensembles. We conclude with a summary of our main findings (Sec. IV).

We use atomic units throughout the rest of this paper, except where indicated otherwise.

## II. RF-DRESSED TWO-LEVEL SYSTEMS

### A. RF-dressing in the adiabatic approximation

We first concentrate on the rf dynamics of the subsystem formed by the intermediate and upper states of our 3-level ladder Rydberg system, states  $|b\rangle$  and  $|c\rangle$ . We thus assume, for the time being, that neither  $|b\rangle$  nor  $|c\rangle$  interact with the lower state of the system,  $|a\rangle$ . Making the rotating wave approximation for the laser field and passing to slowly-varying variables would then reduce the time-dependent Schrödinger equation to

$$\frac{d}{dt} \begin{pmatrix} c_b \\ c_c \end{pmatrix} = \begin{pmatrix} 0 & -i\Omega_c/2 \\ -i\Omega_c/2 & i\Delta_c \end{pmatrix} \begin{pmatrix} c_b \\ c_c \end{pmatrix} \quad (1)$$

if the rf field was absent.  $\Omega_c$  and  $\Delta_c$  are respectively the Rabi frequency [33] (which we assume real) and the detuning of the control laser field coupling the states  $|b\rangle$  and  $|c\rangle$  in the ladder system: Denoting the zero-field energies of these two states by  $w_b$  and  $w_c$  and the angular frequency of the control laser by  $\omega_c$ ,  $\Delta_c = \omega_c - \omega_{cb}$  with  $\omega_{cb} = w_c - w_b$ . The state vector of the system,  $|\Psi(t)\rangle$ , is a linear superposition of the bare states  $|b\rangle$  and  $|c\rangle$  and the functions  $c_b(t)$  and  $c_c(t)$  are the respective probability amplitudes:

$$|\Psi(t)\rangle = c_b(t)|b\rangle + c_c(t)|c\rangle. \quad (2)$$

We write the electric field component of the rf field as

$$\mathcal{E}(t) = \mathcal{E}_{\text{rf}} \sin(\omega_{\text{rf}} t). \quad (3)$$

We assume that the angular frequency  $\omega_{\text{rf}}$  is so much smaller than  $\omega_{bc}$ , and so much smaller than the transition frequencies between  $|b\rangle$  and  $|c\rangle$  and any other unperturbed state, that  $|b\rangle$  and  $|c\rangle$  evolve adiabatically under the effect of this field. Hence, we replace the time-dependent bare states  $\exp(-iw_b t)|b\rangle$  and  $\exp(-iw_c t)|c\rangle$  by the adiabatic states [11, 12, 14, 34]

$$|B(t)\rangle = \exp\left(-i \int^t E_b[\mathcal{E}(t')] dt'\right) |b[\mathcal{E}(t)]\rangle \quad (4)$$

and

$$|C(t)\rangle = \exp\left(-i \int^t E_c[\mathcal{E}(t')] dt'\right) |c[\mathcal{E}(t)]\rangle. \quad (5)$$

In these expressions,  $|b[\mathcal{E}]\rangle$  and  $|c[\mathcal{E}]\rangle$  denote the state vectors which develop adiabatically from the unperturbed states  $|b\rangle$  and  $|c\rangle$  when a static electric field is turned on from 0 to  $\mathcal{E}$ , and  $E_b[\mathcal{E}]$  and  $E_c[\mathcal{E}]$  are the corresponding eigenenergies of the Stark Hamiltonian. The rf field is assumed to be weak enough that, in sufficiently good approximation,  $E_b[\mathcal{E}(t)] = w_b - \alpha_b[\mathcal{E}(t)]^2/2$  and  $E_c[\mathcal{E}(t)] = w_c - \alpha_c[\mathcal{E}(t)]^2/2$ , and moreover that  $|b[\mathcal{E}(t)]\rangle = |b\rangle + \mathcal{E}(t)|b^{(1)}\rangle$  and  $|c[\mathcal{E}(t)]\rangle = |c\rangle + \mathcal{E}(t)|c^{(1)}\rangle$ . The two state vectors  $|b^{(1)}\rangle$  and  $|c^{(1)}\rangle$  are defined by first order perturbation theory, and  $\alpha_b$  and  $\alpha_c$  are the static dipole polarizability of the states  $|b\rangle$  and  $|c\rangle$ . For the applications we have in mind,  $|\alpha_c| \gg |\alpha_b|$ , so that one can take  $E_b[\mathcal{E}(t)] \approx w_b$  and  $|b[\mathcal{E}(t)]\rangle \approx |b\rangle$ , and assume that only the upper state  $|c\rangle$  is significantly perturbed by the rf field. Moreover, we are also considering systems for which  $|b\rangle$  and  $|c^{(1)}\rangle$  have the same parity and therefore are not directly coupled to each other by the control laser field. In these conditions, the time-dependent Schrödinger equation for the rf-dressed system becomes

$$\frac{d}{dt} \begin{pmatrix} c_b \\ c_c \end{pmatrix} = \begin{pmatrix} 0 & -i\Omega_c/2 \\ -i\Omega_c/2 & i[\Delta_c - 2\Sigma_c \sin^2 \omega_{\text{rf}}t] \end{pmatrix} \begin{pmatrix} c_b \\ c_c \end{pmatrix} \quad (6)$$

where

$$\Sigma_c = \alpha_c \mathcal{E}_{\text{rf}}^2/4. \quad (7)$$

Eq. (6) is a system of linear differential equations with periodic coefficients, which is amenable to the Floquet description studied in the following section. The effect of relaxation, which is not taken into account in Eq. (6), will be considered in Sec. II C.

## B. Floquet formalism

### 1. Floquet states

By virtue of the Floquet theorem [25, 29–31], any solution of Eq. (6) can be written as a superposition of fundamental solutions of the form

$$c_b(\epsilon; t) = e^{-i\epsilon t} \sum_{n=-\infty}^{\infty} c_{b,n} e^{-2in\omega_{\text{rf}}t}, \quad (8a)$$

$$c_c(\epsilon; t) = e^{-i\epsilon t} \sum_{n=-\infty}^{\infty} c_{c,n} e^{-2in\omega_{\text{rf}}t}, \quad (8b)$$

where the quasienergy  $\epsilon$  and the coefficients  $c_{b,n}$  and  $c_{c,n}$  are constants. (The fundamental angular frequency is  $2\omega_{\text{rf}}$ , not  $\omega_{\text{rf}}$ , because the time-dependence entirely arises from the

periodic Stark shift of the upper level, which varies at twice the rf frequency.) Replacing  $c_b(t)$  and  $c_c(t)$  by  $c_b(\epsilon; t)$  and  $c_c(\epsilon; t)$  turns Eq. (6) into a time-independent system of algebraic equations for the coefficients  $c_{b,n}$  and  $c_{c,n}$ , namely

$$\frac{\Omega_c}{2}c_{c,n} - 2n\omega_{\text{rf}}c_{b,n} = \epsilon c_{b,n}, \quad (9a)$$

$$\begin{aligned} (\Sigma_c - \Delta_c - 2n\omega_{\text{rf}})c_{c,n} + \frac{\Omega_c}{2}c_{b,n} \\ - \frac{\Sigma_c}{2}(c_{c,n-1} + c_{c,n+1}) = \epsilon c_{c,n}. \end{aligned} \quad (9b)$$

The quasienergies are those values of  $\epsilon$  for which this system has a non-trivial solution. In matrix form, Eqs. (9a) and (9b) read

$$\mathbf{H}_{2\text{F}} \mathbf{c} = \epsilon \mathbf{c}, \quad (10)$$

where  $\mathbf{c}$  is the column vector  $(\dots, c_{b,-1}, c_{b,0}, c_{b,+1}, \dots, c_{c,-1}, c_{c,0}, c_{c,+1}, \dots)^T$  and

$$\mathbf{H}_{2\text{F}} = \begin{pmatrix} \ddots & \vdots & \vdots & \vdots & \vdots & \vdots & \vdots & \vdots & \vdots \\ \cdots & 2\omega_{\text{rf}} & 0 & 0 & \cdots & \Omega_c/2 & 0 & 0 & \cdots \\ \cdots & 0 & 0 & 0 & \cdots & 0 & \Omega_c/2 & 0 & \cdots \\ \cdots & 0 & 0 & -2\omega_{\text{rf}} & \cdots & 0 & 0 & \Omega_c/2 & \cdots \\ \cdots & \vdots & \vdots & \vdots & \cdots & \vdots & \vdots & \vdots & \cdots \\ \cdots & \Omega_c/2 & 0 & 0 & \cdots & \Sigma_c - \Delta_c + 2\omega_{\text{rf}} & -\Sigma_c/2 & 0 & \cdots \\ \cdots & 0 & \Omega_c/2 & 0 & \cdots & -\Sigma_c/2 & \Sigma_c - \Delta_c & -\Sigma_c/2 & \cdots \\ \cdots & 0 & 0 & \Omega_c/2 & \cdots & 0 & -\Sigma_c/2 & \Sigma_c - \Delta_c - 2\omega_{\text{rf}} & \cdots \\ \vdots & \vdots & \vdots & \vdots & \vdots & \vdots & \vdots & \vdots & \ddots \end{pmatrix}. \quad (11)$$

The possible values of the quasienergy are the eigenvalues of  $\mathbf{H}_{2\text{F}}$ , which we denote by  $\epsilon_k$ . Each one corresponds to a particular dressed state of the system, i.e., to a solution of the Schrödinger equation of the form

$$|\Psi_k(t)\rangle = e^{-i\epsilon_k t} \sum_{n=-\infty}^{\infty} e^{-2in\omega_{\text{rf}}t} |\psi_{k,n}\rangle, \quad (12)$$

where the state vectors  $|\psi_{k,n}\rangle$  are time-independent. It follows from the above that  $|\Psi_k(t)\rangle = c_b(\epsilon_k; t)|b\rangle + c_c(\epsilon_k; t)|c\rangle$ . We thus have two equivalent descriptions of the dressed states of the system, namely one in terms of the time-dependent coefficients  $c_b(\epsilon_k; t)$  and  $c_c(\epsilon_k; t)$  and one

in terms of the time-independent vector  $|\Psi_k\rangle\rangle \equiv (|\psi_{k,0}\rangle, |\psi_{k,\pm 1}\rangle, |\psi_{k,\pm 2}\rangle, \dots)^T$  formed by the harmonic components of  $|\Psi_k(t)\rangle$ . (Here and in the following, we use the notation  $|\dots\rangle\rangle$  to represent a column vector of state vectors.) The vector  $\mathbf{c}_k$ , solution of Eq. (10) with  $\epsilon = \epsilon_k$ , is the representation of  $|\Psi_k\rangle\rangle$  in the basis of the bare Floquet states

$$|b, n\rangle\rangle \equiv (|b\rangle \delta_{in}, i = 0, \mp 1, \mp 2, \dots)^T \quad (13)$$

and

$$|c, n\rangle\rangle \equiv (|c\rangle \delta_{in}, i = 0, \mp 1, \mp 2, \dots)^T. \quad (14)$$

Thus [35]

$$|\Psi_k\rangle\rangle = \sum_{n=-\infty}^{\infty} (c_{b,-n}|b, n\rangle\rangle + c_{c,n}|c, -n\rangle\rangle). \quad (15)$$

The Hamiltonian matrix  $\mathbf{H}_{2F}$  has a four-block structure. Its upper and lower diagonal blocks,  $\mathbf{H}_b$  and  $\mathbf{H}_c$  respectively, are square matrices representing the Hamiltonians of the Floquet manifolds spawned by the bare states  $|b\rangle$  and  $|c\rangle$ . The non-zero elements of the off-diagonal blocks arise from the coupling of the states  $|b\rangle$  and  $|c\rangle$  by the control field, while the off-diagonal elements  $-\Sigma_c/2$  of  $\mathbf{H}_c$  arise from the coupling of the state  $|c\rangle$  with itself via the absorption or stimulated emission of two rf photons. The rf field thus mixes the different vectors  $|c, n\rangle\rangle$  with each other. By contrast, the matrix  $\mathbf{H}_b$  is diagonal since we neglect the dressing of the state  $|b\rangle$  by the rf field.

It is useful to diagonalize the matrix  $\mathbf{H}_c$ , which can be done by transforming the basis from  $\{|b, n\rangle\rangle, |c, n\rangle\rangle, n = 0, \pm 1, \pm 2, \dots\}$  to  $\{|b', n\rangle\rangle, |c', n\rangle\rangle, n = 0, \pm 1, \pm 2, \dots\}$ , with  $|b', n\rangle\rangle \equiv |b, n\rangle\rangle$  and

$$|c', n\rangle\rangle = \sum_{m=-\infty}^{\infty} J_{n-m} \left( \frac{\Sigma_c}{2\omega_{\text{rf}}} \right) |c, m\rangle\rangle, \quad (16)$$

where  $J_p(x)$  is the  $p$ -th order Bessel function of the first kind [25]. Under this change of basis, the matrix representing the Hamiltonian becomes

$$\mathbf{H}'_{2\text{F}} = \begin{pmatrix} \ddots & \vdots & \vdots & \vdots & \vdots & \vdots & \vdots & \vdots & \vdots \\ \cdots & 2\omega_{\text{rf}} & 0 & 0 & \cdots & \Omega_c J_0/2 & \Omega_c J_{+1}/2 & \Omega_c J_{+2}/2 & \cdots \\ \cdots & 0 & 0 & 0 & \cdots & \Omega_c J_{-1}/2 & \Omega_c J_0/2 & \Omega_c J_{+1}/2 & \cdots \\ \cdots & 0 & 0 & -2\omega_{\text{rf}} & \cdots & \Omega_c J_{-2}/2 & \Omega_c J_{-1}/2 & \Omega_c J_0/2 & \cdots \\ \cdots & \vdots & \vdots & \vdots & \cdots & \vdots & \vdots & \vdots & \cdots \\ \cdots & \Omega_c J_0/2 & \Omega_c J_{-1}/2 & \Omega_c J_{-2}/2 & \cdots & \Sigma_c - \Delta_c + 2\omega_{\text{rf}} & 0 & 0 & \cdots \\ \cdots & \Omega_c J_{+1}/2 & \Omega_c J_0/2 & \Omega_c J_{-1}/2 & \cdots & 0 & \Sigma_c - \Delta_c & 0 & \cdots \\ \cdots & \Omega_c J_{+2}/2 & \Omega_c J_{+1}/2 & \Omega_c J_0/2 & \cdots & 0 & 0 & \Sigma_c - \Delta_c - 2\omega_{\text{rf}} & \cdots \\ \vdots & \vdots & \vdots & \vdots & \vdots & \vdots & \vdots & \vdots & \ddots \end{pmatrix}, \quad (17)$$

where  $J_p$ ,  $p = 0, \pm 1, \dots$ , denotes  $J_p(\Sigma_c/2\omega_{\text{rf}})$ . Neither the quasienergies nor the diagonal elements of the Hamiltonian matrix are affected by this change of basis. We see that in the absence of the control field, i.e., for  $\Omega_c = 0$ , the vectors  $|b', n\rangle\rangle$  and  $|c', m\rangle\rangle$  describe the Floquet sidebands of the states  $|b\rangle$  and  $|c\rangle$ , respectively. When  $\Omega_c \neq 0$ , the sidebands of  $b$  are coupled to those of  $c$  by the off-diagonal blocks of  $\mathbf{H}'_{2\text{F}}$ , the strength of the coupling between the  $n$ -th side band of  $b$  and the  $m$ -th side band of  $c$  being proportional to  $|J_{m-n}(\Sigma_c/2\omega_{\text{rf}})|$  [13].

## 2. Quasienergy spectrum

$\mathbf{H}_{2\text{F}}$  and  $\mathbf{H}'_{2\text{F}}$  reduce to the same diagonal matrix in the absence of control field, i.e., for  $\Omega_c = 0$ . It follows from Eq. (17) that their spectrum is a double comb of quasienergies: When  $\Omega_c = 0$ , any quasienergy  $\epsilon_k$  is equal either to  $\epsilon_{b,n}^{(0)}$  or to  $\epsilon_{c,n}^{(0)}$  for some value of  $n$ , where

$$\epsilon_{b,n}^{(0)} = 2n\omega_{\text{rf}}, \quad (18\text{a})$$

$$\epsilon_{c,n}^{(0)} = \Sigma_c - \Delta_c + 2n\omega_{\text{rf}}. \quad (18\text{b})$$

The corresponding dressed states,  $|\Psi_k\rangle\rangle$ , are either  $|b', n\rangle\rangle$  or  $|c', n\rangle\rangle$ , respectively. Each of the quasienergies is thus associated with an energy sideband of either state  $|b\rangle$  or state  $|c\rangle$ . The sidebands of  $|b\rangle$  are located at the energies  $E_{b,n}^{(0)} = w_b + \epsilon_{b,n}^{(0)} = w_b + 2n\omega_{\text{rf}}$ ,  $n = 0, \pm 1, \dots$ , and those of  $|c\rangle$  at the energies  $E_{c,n}^{(0)} = w_b + \omega_c + \epsilon_{c,n}^{(0)} = w_c + \Sigma_c + 2n\omega_{\text{rf}}$ ,  $n = 0, \pm 1, \dots$  — see Fig. 1(a). As should be expected when  $\Omega_c = 0$ , the sideband energies  $E_{b,n}^{(0)}$  and  $E_{c,n}^{(0)}$



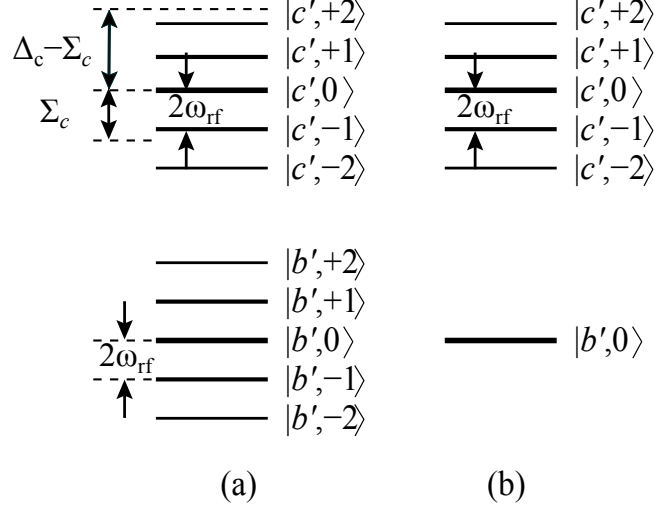


FIG. 1: (a) The manifold structure of the dressed 2-level system. The energy separation between adjacent sidebands is  $2\omega_{\text{rf}}$ . The energy of state  $|c\rangle$  is Stark shifted by the rf field by an amount  $\Sigma_c$ . The effective detuning from resonance of the laser field coupling the two states is thus  $\Delta_c - \Sigma_c$ . (b) The manifold structure in the  $N$ -level approximation: the sidebands of state  $|b\rangle$  are neglected and the interaction between the two manifolds reduces to the interaction of the single state  $|b\rangle$  with the  $N$  states forming the  $c$  manifold.

do not depend on the frequency of the control laser. However, the quasienergies of the  $\epsilon_{c,n}^{(0)}$ -manifold of quasienergies change with the detuning  $\Delta_c$ , with the consequence that this manifold crosses the ( $\omega_c$ -independent)  $\epsilon_{b,n}^{(0)}$ -manifold at  $\Delta_c = \Sigma_c + 2m\omega_{\text{rf}}$ ,  $m = 0, \pm 1, \pm 2, \dots$

The quasienergy spectrum keeps that double comb structure for  $\Omega_c \neq 0$ : any quasienergy  $\epsilon_k$  is equal either to  $\epsilon_{b,n}$  or to  $\epsilon_{c,n}$  for some value of  $n$ , with

$$\epsilon_{b,n} = \epsilon_{b,0} + 2n\omega_{\text{rf}}, \quad (19a)$$

$$\epsilon_{c,n} = \epsilon_{c,0} + 2n\omega_{\text{rf}}, \quad (19b)$$

$\epsilon_{b,0}$  and  $\epsilon_{c,0}$  being such that  $\epsilon_{b,0} \rightarrow \epsilon_{b,0}^{(0)}$  and  $\epsilon_{c,0} \rightarrow \epsilon_{c,0}^{(0)}$  in the limit  $\Omega_c \rightarrow 0$ . Thus  $\epsilon_{b,n} \approx \epsilon_{b,n}^{(0)}$  and  $\epsilon_{c,n} \approx \epsilon_{c,n}^{(0)}$  if the control field is sufficiently weak. However, when  $\Omega_c \neq 0$ , the  $\epsilon_{b,n}$ -manifold and the  $\epsilon_{c,n}$ -manifold are no longer degenerate at  $\Delta_c = \Sigma_c + 2m\omega_{\text{rf}}$ ,  $m = 0, \pm 1, \pm 2, \dots$ . Instead, as illustrated by Fig. 2(a), these two manifolds anticross each other in sequences of avoided crossings.

The gaps and positions of these avoided crossing are determined by the off-diagonal blocks of the Hamiltonian matrix  $H'_{2F}$ . If  $\Sigma_c = 0$ , i.e., if the rf field is vanishingly weak,

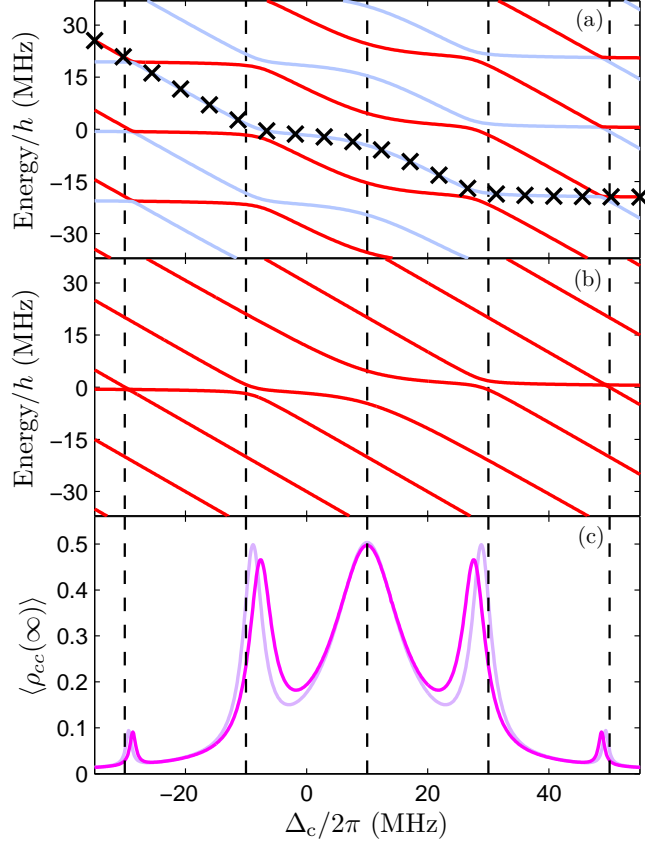


FIG. 2: (color online) The quasienergy spectrum, (a) and (b), and the average population in the upper state at large times ( $t \gg 1/\Gamma_c$ , as defined in Section II C), (c), in an rf-dressed 2-level system.  $\Omega_c/2\pi = 10$  MHz,  $\Sigma_c/2\pi = 10$  MHz,  $\omega_{\text{rf}}/2\pi = 10$  MHz,  $\Gamma_c/2\pi = 1$  MHz and  $\gamma_c = 0$ . (a) and dark pink curve in (c): exact results. (b) and light purple curve in (c): results obtained in the  $N$ -level approximation. Maxima in the population transferred to the upper state occur at the detunings at which the quasienergy curves cross or anticross each other. Differences in the positions and amplitudes of these maxima between the exact results and the  $N$ -level approximation are visible in (c). The crosses represent one of the quasienergy curves predicted by Eqs. (25) and (26).

$J_p(\Sigma_c/2\omega_{\text{rf}}) = \delta_{p0}$ , and these off-diagonal blocks are the unit matrix multiplied by  $\Omega_c/2$ . In this case, the system is equivalent to an infinite set of non-interacting two-level systems. One then has

$$\epsilon_{b,n} = -\frac{\Delta_c}{2} \pm \frac{1}{2} \sqrt{\Delta_c^2 + \Omega_c^2} + 2n\omega_{\text{rf}}, \quad (20a)$$

$$\epsilon_{c,n} = -\frac{\Delta_c}{2} \mp \frac{1}{2} \sqrt{\Delta_c^2 + \Omega_c^2} + 2n\omega_{\text{rf}}, \quad (20b)$$

where the upper signs apply for  $\Delta_c > 0$  and the lower signs for  $\Delta_c < 0$ . The states interchange character at  $\Delta_c = 0$ . However, since in the absence of the rf field Floquet harmonic components of different  $n$  values are not coupled to each other, the crossings between the  $b$  and the  $c$  manifolds at  $\Delta_c = 2m\omega_{\text{rf}}$  ( $m \neq 0$ ) are true crossings rather than avoided crossings.

The off-diagonal elements of the off-diagonal blocks are normally non-zero if the rf field is not vanishingly weak, but they rapidly decrease away from the diagonal when  $|\Sigma_c/2\omega_{\text{rf}}| \ll 1$  since  $J_p(\Sigma_c/2\omega_{\text{rf}})$  then goes rapidly to zero when  $|p|$  increases. If one neglects these off-diagonal elements, Eqs. (20a) and (20b) then generalize to  $\epsilon_{b,n} \approx \epsilon_{b,n}^{(1)}$  and  $\epsilon_{c,n} \approx \epsilon_{c,n}^{(1)}$ , with

$$\begin{aligned}\epsilon_{b,n}^{(1)} &= \frac{1}{2} \left( \epsilon_{b,n}^{(0)} + \epsilon_{c,n}^{(0)} \right) \pm \frac{1}{2} \sqrt{\left( \epsilon_{b,n}^{(0)} - \epsilon_{c,n}^{(0)} \right)^2 + \Omega_c^2 J_0^2} \\ &= \frac{1}{2} (\Sigma_c - \Delta_c) \pm \frac{1}{2} \sqrt{(\Sigma_c - \Delta_c)^2 + \Omega_c^2 J_0^2} + 2n\omega_{\text{rf}}\end{aligned}\quad (21)$$

and

$$\begin{aligned}\epsilon_{c,n}^{(1)} &= \frac{1}{2} \left( \epsilon_{b,n}^{(0)} + \epsilon_{c,n}^{(0)} \right) \mp \frac{1}{2} \sqrt{\left( \epsilon_{b,n}^{(0)} - \epsilon_{c,n}^{(0)} \right)^2 + \Omega_c^2 J_0^2} \\ &= \frac{1}{2} (\Sigma_c - \Delta_c) \mp \frac{1}{2} \sqrt{(\Sigma_c - \Delta_c)^2 + \Omega_c^2 J_0^2} + 2n\omega_{\text{rf}}.\end{aligned}\quad (22)$$

The upper signs apply for  $\Delta_c > \Sigma_c$  and the lower signs for  $\Delta_c < \Sigma_c$ . The control laser field thus lifts the degeneracy between the states  $|b', n\rangle$  and  $|c', n\rangle$  at  $\Delta_c = \Sigma_c$  and creates an energy gap approximately equal to  $\Omega_c J_0(\Sigma_c/2\omega_{\text{rf}})$  between  $\epsilon_{b,n}$  and  $\epsilon_{c,n}$ . In Fig. 2(a), this interaction results in conspicuous avoided crossings at  $\Delta_c/(2\pi) \approx 10$  MHz.

The two manifolds formed by the quasienergy curves  $\epsilon_{b,n}^{(1)}$  cross each other at the detunings at which  $\epsilon_{b,n}^{(1)} = \epsilon_{c,n \pm m}^{(1)}$ ,  $m = 1, 2, \dots$ , i.e., at  $\Delta_c = \Delta_{c, \pm m}$  with

$$\Delta_{c, \pm m} = \Sigma_c \pm \sqrt{4m^2\omega_{\text{rf}}^2 - \Omega_c^2 J_0^2}.\quad (23)$$

Therefore these true crossings do not occur exactly at  $\Delta_c = \Sigma_c \pm 2m\omega_{\text{rf}}$ , as would be the case if  $\Omega_c = 0$ , but instead at detunings shifted towards the avoided crossings at  $\Delta_c = \Sigma_c$ . Expanding the square root function to lowest order in  $\Omega_c$ , Eq. (23) gives

$$\Delta_{c, \pm m} \approx \Sigma_c \pm 2m\omega_{\text{rf}} \mp \Omega_c^2 J_0^2 / (4m\omega_{\text{rf}}).\quad (24)$$

This result can also be obtained using perturbation theory.

The degeneracy of the  $\epsilon_{b,n}^{(1)}$  and  $\epsilon_{c,n\pm m}^{(1)}$  quasienergies at  $\Delta_{c,\pm m}$  is lifted by the off-diagonal terms of the off-diagonal blocks of the Hamiltonian matrix  $H'_{2F}$ . For instance, the avoided crossings visible at  $\Delta_c/(2\pi) \approx -10$  MHz and 30 MHz in Fig. 2(a) originate from the terms  $\Omega_c J_{\pm 1}$  in these off-diagonal blocks, which couple the  $|b', n\rangle\rangle$  states to the  $|c', \pm 1\rangle\rangle$  states. Treating each pair of intersecting quasienergies as an isolated two-level system in the vicinity of their intersection and neglecting the terms in  $\Omega_c J_{\pm m}$  with  $m > 1$  in  $H'_{2F}$  yields the improved approximation  $\epsilon_{b,n} \approx \epsilon_{b,n}^{(2)}$  and  $\epsilon_{c,n} \approx \epsilon_{c,n}^{(2)}$ , with

$$\epsilon_{b,n}^{(2)} = \frac{1}{2} \left( \epsilon_{b,n}^{(1)} + \epsilon_{c,n-1}^{(1)} \right) \pm \frac{1}{2} \sqrt{\left( \epsilon_{b,n}^{(1)} - \epsilon_{c,n-1}^{(1)} \right)^2 + \Omega_c^2 J_1^2} \quad (25)$$

and

$$\epsilon_{c,n}^{(2)} = \frac{1}{2} \left( \epsilon_{b,n+1}^{(1)} + \epsilon_{c,n}^{(1)} \right) \mp \frac{1}{2} \sqrt{\left( \epsilon_{b,n+1}^{(1)} - \epsilon_{c,n}^{(1)} \right)^2 + \Omega_c^2 J_1^2}. \quad (26)$$

As in the above, the signs should be chosen so that  $\epsilon_{b,n}^{(2)} \rightarrow \epsilon_{b,n}^{(0)}$  and  $\epsilon_{c,n}^{(2)} \rightarrow \epsilon_{c,n}^{(0)}$  for  $\Omega_c \rightarrow 0$ . One of the resulting quasienergy curves is represented by crosses in Fig. 2(a). As seen from the figure, it reproduces the exact quasienergies well. The only significant differences occur when  $\Delta_c \approx \Delta_{c,\pm m}$  with  $m \geq 2$ , where the approximate quasienergy manifolds  $\epsilon_{b,n}^{(2)}$  and  $\epsilon_{c,n}^{(2)}$  cross rather than anticross each other. The approximation can be improved by taking into account more off-diagonal components of the off-diagonal blocks of  $H'_{2F}$  and further iterating the process leading to Eqs. (25) and (26). The effective Rabi frequency for two quasienergy curves intersecting at  $\Delta_c \approx \Delta_{c,\pm m}$  is  $\Omega_c |J_{\pm m}(\Sigma_c/2\omega_{\text{rf}})|$ . The gap of the corresponding avoided crossing is therefore a decreasing function of  $m$  when, as we have been assuming throughout this discussion,  $|\Sigma_c/(2\omega_{\text{rf}})| \ll 1$ .

Treating the crossings at  $\Delta_c \approx \Delta_{c,\pm 1}$  separately from that at  $\Delta_c = \Sigma_c$  is justified if the former are sufficiently far apart from the latter, namely if  $|\Delta_{c,\pm 1} - \Sigma_c| \gg \max(|\Omega_c J_0|, |\Omega_c J_1|)$ . Given that  $J_0(\Sigma_c/2\omega_{\text{rf}}) \gg J_1(\Sigma_c/2\omega_{\text{rf}})$  when  $\Sigma_c/(2\omega_{\text{rf}}) \ll 1$ , this condition can also be written

$$\left| \frac{\Omega_c J_0}{2\omega_{\text{rf}}} \right| \ll 1. \quad (27)$$

The iterative method outlined above fails when the inequality (27) is violated. The crossings between the manifolds may then occur at different values of  $\Delta_c$  than predicted by Eqs. (23) and (24).

Finally, we note that for weak fields the quasienergies obtained by the iterative method

are consistent with those predicted by perturbation theory, namely, for  $n = 0$  [36],

$$\epsilon_{b,0} \approx - \sum_{n=-\infty}^{\infty} \frac{(\Omega_c J_n/2)^2}{\Sigma_c - \Delta_c - 2n\omega_{\text{rf}}}, \quad (28a)$$

$$\epsilon_{c,0} \approx \Sigma_c - \Delta_c + \sum_{n=-\infty}^{\infty} \frac{(\Omega_c J_n/2)^2}{\Sigma_c - \Delta_c - 2n\omega_{\text{rf}}}. \quad (28b)$$

### 3. The $N$ -level approximation

As seen above, the bare state  $|b\rangle$  turns into a manifold of sideband states when the system is described in the Floquet formalism. The different states of this manifold are not directly coupled to each other by the rf field under our assumption that the dressing of state  $|b\rangle$  by this field is negligible; however, they interact with each other indirectly, through their coupling with the harmonic components of state  $|c\rangle$  by the control laser field. Neglecting the manifold structure of state  $|b\rangle$  amounts to setting  $c_{b,n} \equiv 0$  for  $n \neq 0$  in Eq. (8a) and to reducing the Hamiltonian matrix  $\mathbf{H}'_{2\text{F}}$  to the matrix

$$\tilde{\mathbf{H}}'_{2\text{F}} = \begin{pmatrix} 0 & \cdots & \Omega_c J_{-1}/2 & \Omega_c J_0/2 & \Omega_c J_{+1}/2 & \cdots \\ \vdots & \ddots & \vdots & \vdots & \vdots & \cdots \\ \Omega_c J_{-1}/2 & \cdots & \Sigma_c - \Delta_c + 2\omega_{\text{rf}} & 0 & 0 & \cdots \\ \Omega_c J_0/2 & \cdots & 0 & \Sigma_c - \Delta_c & 0 & \cdots \\ \Omega_c J_{+1}/2 & \cdots & 0 & 0 & \Sigma_c - \Delta_c - 2\omega_{\text{rf}} & \cdots \\ \vdots & \vdots & \vdots & \vdots & \vdots & \ddots \end{pmatrix}. \quad (29)$$

We refer to this approximation as the  $N$ -level approximation, in view of the fact that the matrix  $\tilde{\mathbf{H}}'_{2\text{F}}$  is effectively the Hamiltonian of a system consisting of a single state  $|b', 0\rangle \equiv |b\rangle$  interacting with a manifold of  $N$  independent states  $|c', n\rangle$ ,  $N \rightarrow \infty$  — see Fig. 1(b). As mentioned in the Introduction, this approximation has often been made in studies of the interaction of low-lying states with rf-dressed Rydberg states.

The corresponding quasienergies are the eigenvalues  $\tilde{\epsilon}_k$  of the matrix  $\tilde{\mathbf{H}}'_{2\text{F}}$ . An example of the resulting spectrum is shown in Fig. 2(b). Proceeding as in Sec. II B 2, one finds that for  $\Omega_c = 0$  the corresponding quasienergies are equal either to  $\tilde{\epsilon}_b^{(0)} \equiv 0$  or to  $\tilde{\epsilon}_{c,n}^{(0)} \equiv \epsilon_{c,n}^{(0)}$  for some value of  $n$ , whereas for  $\Omega_c \neq 0$  and  $|\Sigma_c/(2\omega_{\text{rf}})| \ll 1$ , they are approximately equal either to  $\tilde{\epsilon}_b^{(1)} \equiv \epsilon_{b,0}^{(1)}$ , to  $\tilde{\epsilon}_{c,0}^{(1)} \equiv \epsilon_{c,0}^{(1)}$ , or to  $\tilde{\epsilon}_{c,n}^{(1)} \equiv \epsilon_{c,n}^{(0)}$  ( $n \neq 0$ ). In the latter case, the  $c$ -manifold intersects the  $b$ -quasienergy curve at values of  $\Delta_c$  for which  $\tilde{\epsilon}_b^{(1)} = \tilde{\epsilon}_{c,n}^{(1)}$  for some value of  $n$ . However,

these intersections normally occur at different detunings than found in Sec. II B 2, since in general  $\tilde{\epsilon}_{c,n}^{(1)} \neq \epsilon_{c,n}^{(1)}$  when  $n \neq 0$ . Instead, the crossings occur at  $\Delta_c = \tilde{\Delta}_{c,\pm m}$  where

$$\tilde{\Delta}_{c,\pm m} = \Sigma_c \pm 2m\omega_{\text{rf}} \mp \Omega_c^2 J_0^2 / (8m\omega_{\text{rf}}). \quad (30)$$

Comparing this result with Eq. (24), we see that within the  $N$ -level approximation the shift of the crossings from their zero- $\Omega_c$  positions is about half the correct value [37].

### C. Dressed state dynamics and relaxation

Being entirely based on Eq. (6), the analysis developed in Sec. II B neglects both the frequency width of the control laser and the energy width of the states  $|b\rangle$  and  $|c\rangle$ . The corresponding time evolution of the system is purely oscillatory, with population transferred to-and-fro between  $|b\rangle$  and  $|c\rangle$  without any damping. The evolution would be a pure Rabi flopping of characteristic angular frequency  $(\Delta_c^2 + \Omega_c^2)^{1/2}$  in the absence of the rf field. The oscillation is multimode in the presence of the latter, with Fourier components separated in angular frequency by integer multiples of  $2\omega_{\text{rf}}$ . Eqs. (21) and (22) approximately give the corresponding characteristic frequencies as  $[(\Sigma_c - \Delta_c)^2 + \Omega_c^2 J_0^2]^{1/2} / 2 + 2p\omega_{\text{rf}}$ ,  $p = 0, \pm 1, \pm 2, \dots$

Relaxation modifies this picture. Taking into account the natural width of state  $|c\rangle$ ,  $\Gamma_c$ , and the linewidth of the control laser,  $\gamma_c$ , and assuming that  $|c\rangle$  can de-excite only to  $|b\rangle$ , the time evolution of the system is described by the following optical Bloch equations:

$$\dot{\rho}_{bb} = \Gamma_c \rho_{cc} + \frac{i\Omega_c}{2} (\rho_{bc} - \rho_{cb}), \quad (31a)$$

$$\dot{\rho}_{cc} = -\Gamma_c \rho_{cc} + \frac{i\Omega_c}{2} (\rho_{cb} - \rho_{bc}), \quad (31b)$$

$$\begin{aligned} \dot{\rho}_{bc} = & -\left\{ \Gamma_c / 2 + \gamma_c + i \left[ \Delta_c - 2\Sigma_c \sin^2 \omega_{\text{rf}} t \right] \right\} \rho_{bc} \\ & + \frac{i\Omega_c}{2} (\rho_{bb} - \rho_{cc}). \end{aligned} \quad (31c)$$

(Recall that at the moment we study the system formed by states  $|b\rangle$  and  $|c\rangle$  in isolation from state  $|a\rangle$ . We therefore assume, for the time being, that  $|b\rangle$  does not de-excite to a lower state. The finite lifetime of state  $|b\rangle$  will be taken into account in the analysis of the full 3-level ladder system, in Sec. III.) Decoherence dampens the dynamical evolution of the system until the oscillation is purely driven by the rf field. In this steady state, which is reached for  $t \gg 1/\Gamma_c$ , the elements of the density matrix oscillate at integer multiples of the fundamental angular frequency  $2\omega_{\text{rf}}$  about a constant cycle-average.

In the  $N$ -level approximation, we treat each side band of state  $|c\rangle$  as an independent bound state and describe the evolution of the system by optical Bloch equations based on the Hamiltonian matrix  $\tilde{\mathbf{H}}'_{2F}$ , namely

$$\dot{\rho}_{bb} = \Gamma_c \sum_k \rho_{kk} + \frac{i\Omega_c}{2} \sum_k (J_k \rho_{bk} - J_k \rho_{kb}), \quad (32a)$$

$$\begin{aligned} \dot{\rho}_{bk} = & - [\Gamma_c/2 + \gamma_c - i(\Sigma_c - \Delta_c - 2k\omega_{rf})] \rho_{bk} \\ & + \frac{i\Omega_c}{2} \left( \rho_{bb} - \sum_j J_j \rho_{jk} \right), \end{aligned} \quad (32b)$$

$$\dot{\rho}_{jk} = - [\Gamma_c - 2i(j-k)\omega_{rf}] \rho_{jk} + \frac{i\Omega_c}{2} (J_k \rho_{jb} - J_j \rho_{bk}), \quad (32c)$$

with the indexes  $j$  and  $k$  running over all the states forming the  $c$ -manifold. In this approach, the population in state  $|c\rangle$ ,  $\rho_{cc}$ , is defined as  $1 - \rho_{bb}$ , or equivalently, as  $\rho_{cc} = \sum_k \rho_{kk}$ . In contrast to Eqs. (31a–31c), which predict oscillatory populations and coherences, Eqs. (32a–32c) lead to a constant density matrix in the long time limit.

We assume that the atom is initially in state  $|b\rangle$  and calculate the population transferred to state  $|c\rangle$ ,  $\rho_{cc}(t)$ , and its temporal average in the steady state,  $\langle \rho_{cc}(\infty) \rangle$ . We define the latter as

$$\langle \rho_{cc}(\infty) \rangle = \frac{1}{T} \lim_{t \rightarrow \infty} \int_t^{t+T} \rho_{cc}(t') dt', \quad (33)$$

with  $T = 2\pi/(2\omega_{rf})$ . We thus set  $\rho_{bb}$  to 1 and all the other elements of the density matrix to zero at time  $t = 0$  and numerically solve either Eqs. (31a–31c) or Eqs. (32a–32c) from  $t = 0$  to  $t \gg 1/\Gamma_c$ .

How the population transferred to state  $|c\rangle$  varies with the detuning  $\Delta_c$  depends both on the value of  $\Gamma_c$  and on whether the inequality (27) is fulfilled or not. Avoided crossings between quasienergy curves can be treated in isolation when this inequality is fulfilled, and adjacent resonances do not overlap significantly due to the natural width of the upper level when  $\Gamma_c \ll 2\omega_{rf}$ . The variation of  $\langle \rho_{cc}(\infty) \rangle$  in these conditions is exemplified by Fig. 2(c). The results represented respectively by a dark pink curve and by a light purple curve were obtained by solving Eqs. (31a–31c) and Eqs. (32a–32c).

As seen from the figure, the avoided crossings in the dressed state spectrum are associated with strong enhancements of population transfer. The origin of these enhancements is easily understood given that  $\Gamma_c$  and  $\gamma_c$  are both sufficiently small that the evolution of the system is dominated by its dressed states dynamics rather than by relaxation. For the parameters

considered, the dressed atom can be described as a simple two-state system in the vicinity of each avoided crossing. Sufficiently far from any crossing, the dressed states are close to either one of the  $|b', n\rangle$  states or one of the  $|c', n\rangle$  states, with little admixture between the two. At a crossing, however, the interacting dressed states are approximately equal superpositions of  $|b\rangle$  and  $|c\rangle$ . Population transfer is therefore enhanced at each crossing, typically over the range of values of  $\Delta_c$  for which the relevant  $b$ - and  $c$ -dressed states are significantly admixed with each other. Treating the dressed atom as a pure two-state system in the vicinity of each crossing leads to a simple expression for the population transferred to the upper state, i.e., for  $\Delta_c \approx \Sigma_c + 2n\omega_{\text{rf}}$  [36],

$$\langle \rho_{cc}(\infty) \rangle \approx \frac{\Omega_c^2 J_n^2 / 2}{\Gamma_c (\Gamma_c / 2 + \gamma_c) [1 + (\Delta_c - \Sigma_c - 2n\omega_{\text{rf}})^2 / \Gamma_c^2] + \Omega_c^2 J_n^2}. \quad (34)$$

Thus  $\langle \rho_{cc}(\infty) \rangle$  exhibits power-broadened sidebands whose height and width are modulated by the square of the Bessel function factors  $J_n$ . When  $|n|$  is larger than the argument of these Bessel functions, these enhancements decrease in amplitude and their width tends to the natural width of the upper level,  $\Gamma_c$ , for increasing sideband orders. For the parameters of Fig. 2(c), this analysis predicts that the  $n = 0$ ,  $n = \pm 1$  and  $n = \pm 2$  enhancements have an height of 0.50, 0.46 and 0.08, respectively, and a full width at half maximum of 13.3, 3.6 and 1.1 MHz. As can be seen from the figure (dark purple curve), these values are in agreement with the numerical results, although the  $n = 0$  sideband somewhat overlaps the others. (The inequality (27) is fulfilled but marginally here, since  $|\Omega_c J_0| / (2\omega_{\text{rf}}) \approx 0.5$ .)

The picture is the same in the  $N$ -level approximation for the parameters considered. The discrepancy in the position of the enhancements mirrors the differences in the position of the crossings in the quasienergy maps. It can be largely eliminated by a simple  $k$ -dependent shift in the  $\Sigma_c - \Delta_c - 2k\omega_{\text{rf}}$  factor multiplying  $\rho_{bk}$  in Eq. (32b) [37].

The comparison shows that for the parameters considered in Fig. 2, the upper state effectively turns into a manifold of states well described within the  $N$ -level approximation. As mentioned in Sec. II B 2, increasing  $\Omega_c$  eventually results in a break down of this approximation as the states forming the Floquet manifold will start to interact with each other. For sufficiently strong control fields, the resonance sidebands overlap each other and merge with the zeroth order resonance.

How large  $|\Omega_c J_0|$  is relative to  $2\omega_{\text{rf}}$  also impacts on the temporal evolution of the system. When  $|\Omega_c J_0| \ll 2\omega_{\text{rf}}$ , the atom interacts with the laser field as if state  $|c\rangle$  were a manifold



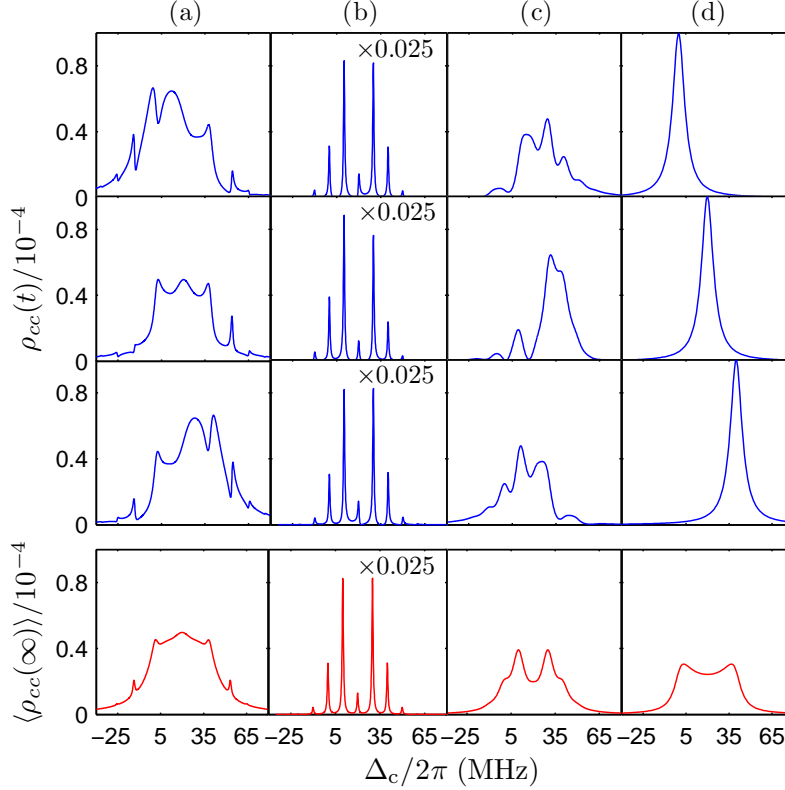


FIG. 3: (color online) The population in the upper state at  $\sin^2 \omega_{\text{rf}} t = 0$  (first row),  $1/2$  (second row) and  $1$  (third row), and its time average (bottom row), in the steady state regime ( $t \gg 1/\Gamma_c$ ).  $\Sigma_c/(2\pi) = 20$  MHz and  $\gamma_c = 0$  in all cases. (a):  $\Omega_c/2\pi = 20$  MHz,  $\Gamma_c/2\pi = 1$  MHz and  $\omega_{\text{rf}}/2\pi = 5$  MHz. (b):  $\Omega_c/2\pi = 0.1$  MHz,  $\Gamma_c/2\pi = 1$  MHz and  $\omega_{\text{rf}}/2\pi = 5$  MHz. (c):  $\Omega_c/2\pi = 0.1$  MHz,  $\Gamma_c/2\pi = 10$  MHz and  $\omega_{\text{rf}}/2\pi = 5$  MHz. (d):  $\Omega_c/2\pi = 0.1$  MHz,  $\Gamma_c/2\pi = 10$  MHz and  $\omega_{\text{rf}}/2\pi = 0.01$  MHz.  $\Sigma_c/(2\pi) = 20$  MHz and  $\gamma_c = 0$  in all cases.  $\rho_{cc}$  is multiplied by a factor of 0.025 in column (b).

of stationary states. In the opposite limit, the rf field changes slowly on the time scale on which the states  $|b\rangle$  and  $|c\rangle$  interact with each other. This interaction then occurs as if the rf field was static at any instant. In this case, the Stark shift due to the rf field is expected to make the population in the state  $|c\rangle$  oscillate periodically.

Columns (a) and (b) of Fig. 3 compare instantaneous and cycle-average values of  $\rho_{cc}$  in the steady state regime for two different values of  $\Omega_c$ . In column (a),  $|\Omega_c J_0|/(2\omega_{\text{rf}}) \approx 0.4$ . This value is insufficiently small for the  $N$ -state picture to hold well, which leads to a clear oscillation in the population in the state  $|c\rangle$ . In column (b),  $|\Omega_c J_0|/(2\omega_{\text{rf}}) \approx 0.002$ , which

fulfills the condition (35):  $\rho_{cc}$  is almost constant in time. The resonance sidebands are also much better marked than in column (a) because of the much smaller power broadening.

The population in the state  $|c\rangle$  also depends on the time scale of the relaxation mechanisms. Well defined enhancement sidebands are not expected unless spontaneous decay is slow compared to the oscillation of the rf field, i.e., unless [13]

$$\Gamma_c \ll 2\omega_{\text{rf}}. \quad (35)$$

This inequality also expresses the requirement that adjacent sidebands, which are separated roughly by  $2\omega_{\text{rf}}$ , do not overlap due to the the natural linewidth of the resonance,  $\Gamma_c$ . The role of the lifetime of the state  $|c\rangle$  is illustrated by column (c) of Fig. 3, which was calculated for the same parameters as column (b) apart for  $\Gamma_c$ : while  $\Gamma_c \ll 2\omega_{\text{rf}}$  in column (b),  $\Gamma_c = 2\omega_{\text{rf}}$  in column (c). In the latter case the sidebands partly overlap each other and the population in the state  $|c\rangle$  oscillates markedly.

Finally, column (d) of Fig. 3 shows the time evolution of  $\rho_{cc}$  for the same parameters as in column (c) apart that  $2\omega_{\text{rf}}$  is much smaller than both  $\Gamma_c$  and  $\Delta_c$ . The  $N$ -level picture is now invalid and there is no sign of sidebands. Instead, the profile of  $\rho_{cc}$  is a single peak of width  $\Gamma_c$  following the instantaneous position of state  $|c\rangle$  as this state is periodically Stark-shifted by the rf field [13].

### III. RF-DRESSED THREE-LEVEL SYSTEMS

#### A. General formulation

We now take into account the coupling of state  $|b\rangle$  to state  $|a\rangle$  by the probe laser field and allow state  $|b\rangle$  to de-excite to state  $|a\rangle$ , which is assumed to be stable (Fig. 4). We proceed as in Sec. II A and, ignoring relaxation at first, write the state vector of the atom as

$$|\Psi(t)\rangle = c_a(t)|a\rangle + c_b(t)|b\rangle + c_c(t)|c\rangle, \quad (36)$$

with the amplitudes  $c_a(t)$ ,  $c_b(t)$ ,  $c_c(t)$  satisfying the equation

$$\frac{d}{dt} \begin{pmatrix} c_a \\ c_b \\ c_c \end{pmatrix} = \begin{pmatrix} 0 & -i\Omega_p/2 & 0 \\ -i\Omega_p/2 & i\Delta_p & -i\Omega_c/2 \\ 0 & -i\Omega_c/2 & i[\Delta_R - 2\Sigma_c \sin^2 \omega_{\text{rf}}t] \end{pmatrix} \begin{pmatrix} c_a \\ c_b \\ c_c \end{pmatrix}. \quad (37)$$

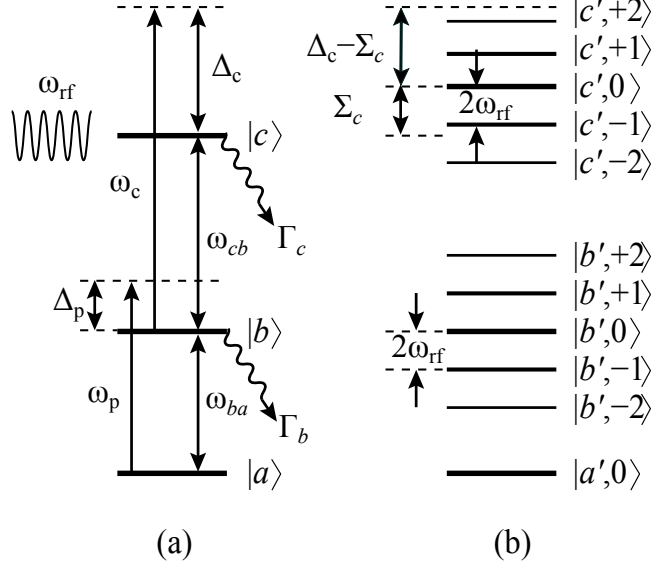


FIG. 4: (a) Schematic of the rf-dressed three-level Rydberg system. The probe laser (angular frequency  $\omega_p$ ) couples the states  $|a\rangle$  and  $|b\rangle$ , while the control laser (angular frequency  $\omega_c$ ) couples the states  $|b\rangle$  and  $|c\rangle$ . The energy of the latter is modulated by the rf field (angular frequency  $\omega_{rf}$ ). The detunings of these two laser fields from the respective transition frequencies are  $\Delta_p$  and  $\Delta_c$ . The state  $|c\rangle$  decays to the state  $|b\rangle$ , and the state  $|b\rangle$  to the state  $|a\rangle$ . (b) The manifold structure of the states  $|b\rangle$  and  $|c\rangle$  induced by the rf field. The energy separation between adjacent sidebands is  $2\omega_{rf}$ . The rf field also shifts the energy of state  $|c\rangle$  by an amount  $\Sigma_c$ ; the effective detuning of the control field is thus  $\Delta_c - \Sigma_c$ .

Following the same analysis as in Sec. II B, we formulate the problem in terms of the Floquet Hamiltonian

$$H_{3F} = \begin{pmatrix} A & \Omega_p & 0 \\ \Omega_p^\dagger & B & \Omega_c \\ 0 & \Omega_c^\dagger & C \end{pmatrix}, \quad (38)$$

where

$$A = \text{diag}(\dots, 2\omega_{rf}, 0, -2\omega_{rf}, \dots), \quad (39a)$$

$$\Omega_p = \text{diag}(\dots, \frac{\Omega_p}{2}, \frac{\Omega_p}{2}, \frac{\Omega_p}{2}, \dots), \quad (39b)$$

and

$$\begin{pmatrix} B & \Omega_c \\ \Omega_c^\dagger & C \end{pmatrix} = H_{2F} - \Delta_p \begin{pmatrix} 1 & 0 \\ 0 & 1 \end{pmatrix}. \quad (40)$$

Generalizing the discussion of last section, the corresponding Floquet states are described by time-independent vectors  $|\Psi_k\rangle\rangle$  which can be written in terms of the vectors  $|a, n\rangle\rangle \equiv (|a\rangle \delta_{in}, i = 0, \mp 1, \mp 2, \dots)^T$  and of the vectors  $|b, n\rangle\rangle$  and  $|c, n\rangle\rangle$  defined by Eqs. (13) and (14):

$$|\Psi_k\rangle\rangle = \sum_{n=-\infty}^{\infty} (c_{a,-n}|a, n\rangle\rangle + c_{b,-n}|b, n\rangle\rangle + c_{c,-n}|c, n\rangle\rangle). \quad (41)$$

As before, the C-block of  $\mathbf{H}_{3\text{F}}$  can be diagonalized by a change of basis transforming the matrix  $\mathbf{H}_{2\text{F}}$  into the matrix  $\mathbf{H}'_{2\text{F}}$  defined by Eq. (17). The change transforms the matrix  $\mathbf{H}_{3\text{F}}$  into the matrix  $\mathbf{H}'_{3\text{F}}$  differing from  $\mathbf{H}_{3\text{F}}$  by the replacement of  $\mathbf{H}_{2\text{F}}$  by  $\mathbf{H}'_{2\text{F}}$ . It does not affect the spectrum of quasienergy. Making the  $N$ -level approximation further reduces  $\mathbf{H}'_{3\text{F}}$  to

$$\tilde{\mathbf{H}}'_{3\text{F}} = \begin{pmatrix} 0 & \Omega_{\text{p}}/2 & \cdots & 0 & 0 & 0 & \cdots \\ \Omega_{\text{p}}/2 & -\Delta_{\text{p}} & \cdots & \Omega_{\text{c}}J_{-1}/2 & \Omega_{\text{c}}J_0/2 & \Omega_{\text{c}}J_{+1}/2 & \cdots \\ 0 & \vdots & \ddots & \vdots & \vdots & \vdots & \cdots \\ 0 & \Omega_{\text{c}}J_{-1}/2 & \cdots & \Sigma_{\text{c}} - \Delta_{\text{R}} + 2\omega_{\text{rf}} & 0 & 0 & \cdots \\ 0 & \Omega_{\text{c}}J_0/2 & \cdots & 0 & \Sigma_{\text{c}} - \Delta_{\text{R}} & 0 & \cdots \\ 0 & \Omega_{\text{c}}J_{+1}/2 & \cdots & 0 & 0 & \Sigma_{\text{c}} - \Delta_{\text{R}} - 2\omega_{\text{rf}} & \cdots \\ \vdots & \vdots & \vdots & \vdots & \vdots & \vdots & \ddots \end{pmatrix}. \quad (42)$$

The optical Bloch equations for the 3-state system with rf-modulation can be written as

$$\dot{\rho}_{aa} = \Gamma_b \rho_{bb} + \frac{i\Omega_p}{2}(\rho_{ab} - \rho_{ba}), \quad (43a)$$

$$\begin{aligned} \dot{\rho}_{bb} = & -\Gamma_b \rho_{bb} + \Gamma_c \rho_{cc} - \frac{i\Omega_p}{2}(\rho_{ab} - \rho_{ba}) \\ & + \frac{i\Omega_c}{2}(\rho_{bc} - \rho_{cb}), \end{aligned} \quad (43b)$$

$$\dot{\rho}_{cc} = -\Gamma_c \rho_{cc} - \frac{i\Omega_c}{2}(\rho_{bc} - \rho_{cb}), \quad (43c)$$

$$\begin{aligned} \dot{\rho}_{ab} = & -(i\Delta_p + \frac{\Gamma_b}{2} + \gamma_p)\rho_{ab} \\ & - \frac{i\Omega_p}{2}(\rho_{bb} - \rho_{aa}) + \frac{i\Omega_c}{2}\rho_{ac}, \end{aligned} \quad (43d)$$

$$\begin{aligned} \dot{\rho}_{bc} = & -(i\Delta_c - 2i\Sigma_c \sin^2 \omega_{\text{rf}}t + \frac{\Gamma_b + \Gamma_c}{2} + \gamma_p + \gamma_c)\rho_{bc} \\ & - \frac{i\Omega_c}{2}(\rho_{cc} - \rho_{bb}) - \frac{i\Omega_p}{2}\rho_{ac}, \end{aligned} \quad (43e)$$

$$\begin{aligned} \dot{\rho}_{ac} = & -(i\Delta_p + i\Delta_c - 2i\Sigma_c \sin^2 \omega_{\text{rf}}t + \frac{\Gamma_c}{2} + \gamma_c)\rho_{ac} \\ & + \frac{i\Omega_c}{2}\rho_{ab} - \frac{i\Omega_p}{2}\rho_{bc}. \end{aligned} \quad (43f)$$

As in Sec. II,  $\Gamma_c$  and  $\gamma_c$  denote the natural width of state  $|c\rangle$  and the linewidth of the control laser.  $\Gamma_b$  and  $\gamma_p$ , which were not introduced in Sec. II, are the corresponding quantities for state  $|b\rangle$  and the probe laser (Fig. 4). Correspondingly, the optical Bloch equations in the

$N$ -level approximation now read

$$\dot{\rho}_{aa} = \Gamma_b \rho_{bb} + \frac{i\Omega_p}{2}(\rho_{ab} - \rho_{ba}), \quad (44a)$$

$$\begin{aligned} \dot{\rho}_{bb} = & -\Gamma_b \rho_{bb} - \frac{i\Omega_p}{2}(\rho_{ab} - \rho_{ba}) \\ & + \Gamma_c \sum_k \rho_{kk} + \frac{i\Omega_c}{2} \sum_k (J_k \rho_{bk} - J_k \rho_{kb}), \end{aligned} \quad (44b)$$

$$\begin{aligned} \dot{\rho}_{ab} = & -\left(\frac{\Gamma_b}{2} + \gamma_p + i\Delta_p\right) \rho_{ab} + \frac{i\Omega_p}{2}(\rho_{aa} - \rho_{bb}) \\ & + \frac{i\Omega_c}{2} \sum_k J_k \rho_{ak}, \end{aligned} \quad (44c)$$

$$\begin{aligned} \dot{\rho}_{ak} = & -\left[\frac{\Gamma_c}{2} + \gamma_p + \gamma_c + i(\Delta_p + \Delta_c - \Sigma_c + 2k\omega_{rf})\right] \rho_{ak} \\ & - \frac{i\Omega_p}{2} \rho_{bk} + \frac{i\Omega_c J_k}{2} \rho_{ab}, \end{aligned} \quad (44d)$$

$$\begin{aligned} \dot{\rho}_{bk} = & -\left[\frac{\Gamma_b + \Gamma_c}{2} + \gamma_c + i(\Delta_c - \Sigma_c + 2k\omega_{rf})\right] \rho_{bk} \\ & + \frac{i\Omega_c}{2} \left(\rho_{bb} - \sum_j J_j \rho_{jk}\right) - \frac{i\Omega_p}{2} \rho_{ak}, \end{aligned} \quad (44e)$$

$$\dot{\rho}_{jk} = -[\Gamma_c - 2i(j-k)\omega_{rf}] \rho_{jk} + \frac{i\Omega_c}{2}(J_k \rho_{jb} - J_j \rho_{bk}), \quad (44f)$$

with the indexes  $j$  and  $k$  running over all the components of the Floquet manifold of state  $|c\rangle$ . These equations are to the Hamiltonian  $\tilde{\mathbf{H}}'_{3F}$  what Eqs. (43a–43f) are to the Hamiltonians  $\mathbf{H}_{3F}$  and  $\mathbf{H}'_{3F}$ . As in the 2-state case, the solutions of Eqs. (44a–44f) tend to constants in the long time limit, whereas those of Eqs. (43a–43f) tend to a steady state in which the elements of the density matrix oscillate at a fundamental angular frequency  $2\omega_{rf}$ . In either case, the absorption coefficient for the probe beam is given by the equation

$$\alpha = -k_p \text{Im} \left[ \frac{2\pi\mathcal{N}|\mathbf{d}_{ba} \cdot \hat{\epsilon}_p|^2}{\epsilon_0 \hbar \Omega_p} \langle \rho_{ba}(\infty) \rangle_{\text{av}} \right], \quad (45)$$

where  $k_p$  is the wave number of the probe field,  $\mathcal{N}$  is the number density of the atoms forming the medium,  $\mathbf{d}_{ba}$  is the matrix element of the dipole operator between the states  $|a\rangle$  and  $|b\rangle$ ,  $\hat{\epsilon}_p$  is the polarization vector of the probe field,  $\epsilon_0$  is the permittivity of free space, and  $\langle \rho_{ba}(\infty) \rangle_{\text{av}}$  denotes the average value of  $\rho_{ba}$  in the stationary regime. For a cold atomic ensemble,  $\langle \rho_{ba}(\infty) \rangle_{\text{av}} \equiv \langle \rho_{ba}(\infty) \rangle$ , with

$$\langle \rho_{ba}(\infty) \rangle = \frac{1}{T} \lim_{t \rightarrow \infty} \int_t^{t+T} \rho_{ba}(t') dt'. \quad (46)$$

For a thermal ensemble where the Doppler effect must be taken into account,  $\langle \rho_{ba}(\infty) \rangle_{\text{av}}$  is the average of  $\langle \rho_{ba}(\infty) \rangle$  over the Maxwellian distribution of velocity of the atoms.

## B. Absorption sidebands and induced sidebands

### 1. Weak control fields

A representative section of the quasienergy spectrum of the full Floquet Hamiltonian is shown in Fig. 5(a) for a case where the control laser is sufficiently weak that the inequality (27) is fulfilled. The horizontal line interrupted by avoided crossings indicates the quasienergy of the zeroth order Floquet sideband of state  $|a\rangle$ . The oblique lines arise either from the sidebands of the state  $|b\rangle$  or from those of the state  $|c\rangle$ , as indicated in the caption. The  $b$ - and  $c$ -quasienergy manifolds run parallel to each other in Fig. 5(a), although they intersect in Fig. 2(a), because the parameter varied in Fig. 5 is the detuning of the probe field while that varied in Fig. 2 is the detuning of the control field. The latter is actually set to zero in these calculations, which means, in view of the Stark shift of state  $|c\rangle$ , that the control laser is off resonance. The quasienergy spectrum obtained in the  $N$ -level approximation is shown in Fig. 5(b), for comparison. The absorption profile for a cold atom ensemble is given in Fig. 5(c). (The quantity represented in Fig. 5(c) is  $\langle \rho_{ba}(\infty) \rangle$ , which is proportional to the absorption coefficient if the atomic motion can be neglected. The maxima of  $\langle \rho_{ba}(\infty) \rangle$  correspond to maxima of absorption.)

The dressed states crossing the horizontal lines all contain the bare state  $|b\rangle$  — i.e., at least one of the  $c_{b,n}$  coefficients is non-zero in Eq. (41). Therefore each of these crossings corresponds to a resonant coupling between this state and the bare state  $|a\rangle$  and may give rise to an enhancement of absorption of the probe field coupling  $|a\rangle$  to  $|b\rangle$ . Fig. 5(c) shows a large enhancement of absorption at the crossing involving the zeroth order sideband of state  $|b\rangle$  (at  $\Delta_p = 0$ ), and smaller enhancements at the other crossings. The enhancement at the crossings with the +1 sideband of  $|c\rangle$  (at 85 MHz) is hardly visible, though, and the enhancements associated with the crossings of the +1 and +2 sidebands of  $|b\rangle$  (at 50 and 100 MHz, respectively) are too small to be seen. These enhancements are weaker compared to those involving the zeroth-order sidebands both because of the scaling of  $\Omega_c$  by the  $J_n$  factors ( $|J_n|$  is much smaller than 1 when  $n \neq 0$  for the parameters of Fig. 5) and because

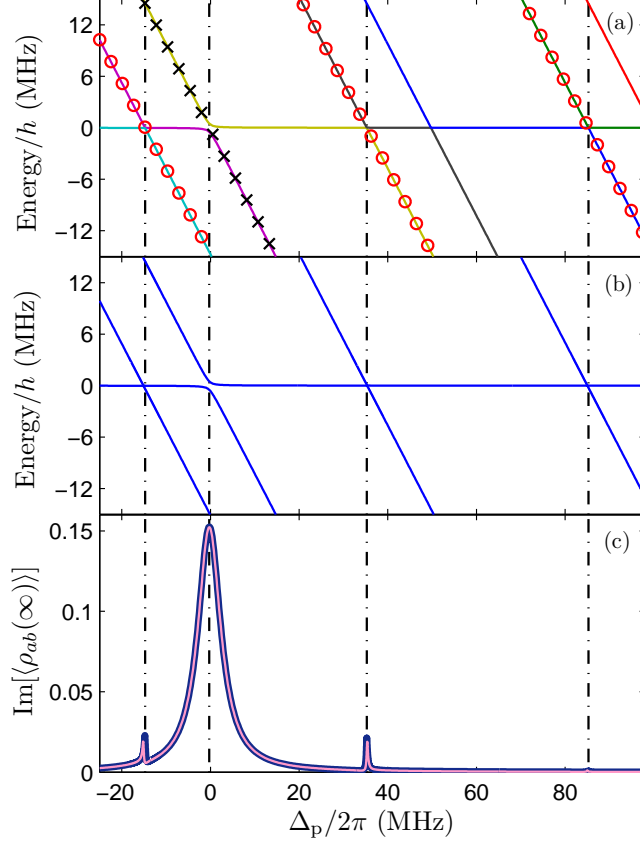


FIG. 5: (color online) The quasienergy spectrum, (a) and (b), and the absorption profile of the probe field, (c), in an rf-dressed 3-level system.  $\Omega_p/2\pi = 1$  MHz,  $\Omega_c/2\pi = 8$  MHz,  $\Sigma_c/2\pi = 35$  MHz,  $\Delta_c/2\pi = 0$  MHz,  $\omega_{\text{rf}}/2\pi = 25$  MHz,  $\Gamma_b/2\pi = 6$  MHz,  $\Gamma_c/2\pi = 0.01$  MHz and  $\gamma_p/2\pi = \gamma_c/2\pi = 0.1$  MHz. (a) and thick dark blue curve in (c): exact results. (b) and thin light pink curve in (c): results in the  $N$ -level approximation. In (a), the crosses identify  $\epsilon_{b,0}$  and the circles  $\epsilon_{c,0}$ ,  $\epsilon_{c,1}$  and  $\epsilon_{c,-1}$ . The other oblique lines correspond to  $\epsilon_{b,n}$ ,  $n \neq 0$ . The horizontal line corresponds to  $\epsilon_{a,0}$ . One may note small differences in the position of the crossings between (a) and (b). Because of the significant Stark shift of the upper state, the control laser is off resonance although  $\Delta_c/2\pi = 0$ , which explains why the absorption profile of the probe field does not exhibit EIT dips.

of the larger energy difference between the respective sidebands (a larger energy difference means a smaller admixture of  $|b\rangle$  into the sidebands of  $|c\rangle$ ). However, as will be seen shortly, significant enhancements may occur at the crossings with the  $n \neq 0$  sidebands of  $b$  for stronger control fields.

Comparing Fig. 5(a) to Fig. 5(b) and the thick blue line to the thin pink line in Fig.



5(c), we see that the  $N$ -level approximation holds well in the present case, as could have been expected since the condition (34) is fulfilled. Because the side bands of the  $b$ -state are neglected in the  $N$ -level approximation, the  $b$ -quasienergy manifold of Fig. 5(a) reduces to a single quasienergy curve in Fig. 5(b). However, the  $c$ -manifold is practically the same in the two spectra. The absorption profile is also very well reproduced in the  $N$ -level approximation for the parameters considered: the two sets of results are almost identical apart for very small differences in the position of the enhancements (noticeable only for the enhancement at  $\Delta_p = -15$  MHz on the scale of the figure) and very small differences in their amplitude.

## 2. Strong control fields

We now increase  $\Omega_c/2\pi$  to 30 and 60 MHz, keeping the other parameters the same as in Fig. 5. The resulting absorption profiles are shown in Figs. 6(a) and 6(b), respectively. As expected from the previous discussion, the  $N$ -level approximation deteriorates as the strength of the control field increases. It is still in rough agreement with the exact result in the case of Fig. 6(a), for which  $\Omega_c$  is smaller, but not much smaller, than  $2\omega_{\text{rf}}$ , although there are differences in the position and the amplitudes of the enhancements. However, when the condition (34) is more strongly violated, the  $N$ -level approximation breaks down completely. There is little agreement with the exact result in Fig. 6(b).

An interesting feature of Fig. 6(a) is the presence of a small enhancement of absorption at  $\Delta_p/2\pi \approx 48$  MHz. This enhancement is not present in the  $N$ -level approximation. It coincides with the crossing of  $|a\rangle$  with the  $+1$  sideband of  $|b\rangle$  in the quasienergy spectrum, at  $2\hbar\omega_{\text{rf}}$  above the main absorption peak (which is concomitant with the crossing of the 0-th order sideband of  $|b\rangle$ .) This feature is more prominent in Fig. 6(b), at  $\Delta_p/2\pi \approx 30$  MHz; the  $+2$  sideband of  $|b\rangle$  is also (barely) visible, at about 80 MHz at this higher power of the control laser. We refer to such sidebands as “induced sidebands”, as they arise from sidebands of  $|b\rangle$  induced by the coupling of this state with the sidebands of  $|c\rangle$  by the control field. (Recall that the rf field is assumed to be too weak to dress state  $|b\rangle$  directly: the  $b$ -manifold originates from the coupling of  $|b\rangle$  to the  $c$ -manifold by the control field, not from the coupling of  $|b\rangle$  to itself by the rf field.)

That the sidebands of  $|a\rangle$  play no role in this absorption profile is shown by the good

agreement between the exact results (thick blue curves) and the results obtained when these sidebands are neglected altogether (green dashed curves).

Before closing, we briefly comment on whether the conditions Eq. (27) and (35) are sufficient to guarantee the validity of the  $N$ -level approximation for a three-state system. Recall that these conditions mean that the oscillations of the rf field are faster than the time scales over which the system evolves under the effect of the control laser field and the spontaneous decay of state  $|c\rangle$ . However, the probe field introduces an additional time scale in the problem: if this field is excessively strong, it will disturb the dynamics of the  $b$ - $c$  system too rapidly for the state  $|c\rangle$  to show a manifold structure. In this case, the Floquet sidebands of state  $|a\rangle$  induced by its coupling to state  $|c\rangle$  can no longer be ignored. Given that the effective Rabi frequency for the coupling of  $|a\rangle$  to  $|c\rangle$  is approximately given by  $\Omega_p\Omega_c/2\Sigma_c$  [38, 39], we expect that the condition

$$\left|\frac{\Omega_p\Omega_c}{2\Sigma_c}\right| \ll 2\omega_{\text{rf}} \quad (47)$$

should be added to the conditions Eq. (27) and (35) for the  $N$ -level approximation to be valid. Should the inequality (47) not be fulfilled, then it is likely that the Floquet sidebands of  $|a\rangle$  need to be taken into account, as well as those of  $|b\rangle$  and  $|c\rangle$ .

### C. EIT in rf-dressed atomic ensembles

#### 1. Cold atomic ensembles

We still assume that the Doppler effect is negligible, as in the last section. However, we now set  $\Delta_p$  to 0 and vary  $\Delta_c$  rather than set  $\Delta_c$  to 0 and vary  $\Delta_p$ . If the rf field was absent, the control laser field would couple the states  $|b\rangle$  and  $|c\rangle$  resonantly at  $\Delta_c = 0$ , which would be accompanied by a dip in  $\text{Im}[\langle\rho_{ab}(\infty)\rangle]$ . (This is the well known EIT absorption window at  $\Delta_p = 0$  [1].) In the presence of the rf field, this dip is displaced to  $\Delta_c = \Sigma_c$ , due to the ac Stark shift of  $|c\rangle$ , and splits into multiple sidebands.

EIT with rf modulation is illustrated by Fig. 7. These results were calculated for the same values of  $\Omega_p$ ,  $\Sigma_c$ ,  $\omega_{\text{rf}}$ ,  $\Gamma_b$ ,  $\Gamma_c$ ,  $\gamma_p$  and  $\gamma_c$  as in Figs. 3 and 5. The probe Rabi frequency,  $\Omega_p/2\pi$ , increases from 8 MHz in Fig. 7(a) to 30 MHz in Fig. 7(b) and to 60 MHz in Fig. 7(c). As seen from the figure, the rf field creates transmission sidebands on either side of the main EIT feature. Since  $\Delta_p$  is set to zero and the frequency of the control field is varied,

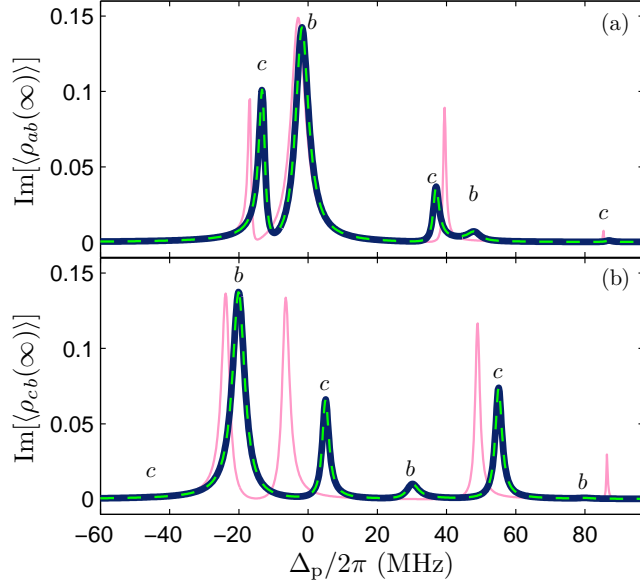


FIG. 6: (color online) The probe absorption in the same rf-dressed 3-level system as in Fig. 5 but for stronger control fields for which the  $N$ -level approximation is inaccurate.  $\Omega_c/2\pi = 30$  MHz in (a) and 60 MHz in (b). Thick blue solid curves: results obtained by solving the full optical Bloch equations, Eqs. (43a–43f). Thin pink solid curves: results obtained in the  $N$ -level approximation, Eqs. (44a–44f). Dashed green curves: results obtained by adding the sidebands of state  $|b\rangle$ , but not those of state  $|a\rangle$ , to the  $N$ -level approximation. The enhancements associated with crossings between the lower state and the intermediate state manifold are identified by the letter  $b$  between the lower state and the Rydberg state manifold by the letter  $c$ .

these sidebands occur at the values of  $\Delta_c$  at which the  $c$ -quasienergy manifold intersects the zeroth-order quasienergy sideband of the state  $|b\rangle$ . In the weak control case of Fig. 7(a), they manifest as narrow dips regularly spaced by  $2\omega_{\text{rf}}$  [40]. Apart for minor differences in the depth, the  $N$ -state approximation reproduces these features very well (the thick blue curve to the thin pink curve). The absorption profile is thus well explained by the model in which the upper state simply splits into a comb of Floquet states, each one interacting with the intermediate state independently from the others. However, this picture changes when  $\Omega_c$  approaches or exceeds  $2\omega_{\text{rf}}$  — see, respectively, Fig. 7(b) and (c): the EIT dips broaden and shift towards the zeroth-order sideband when  $\Omega_c$  increases, and the absorption profile first acquires a peak-and-trough structure and then changes into a series of absorption peaks (rather than absorption dips) superimposed on a slowly varying background. These peaks

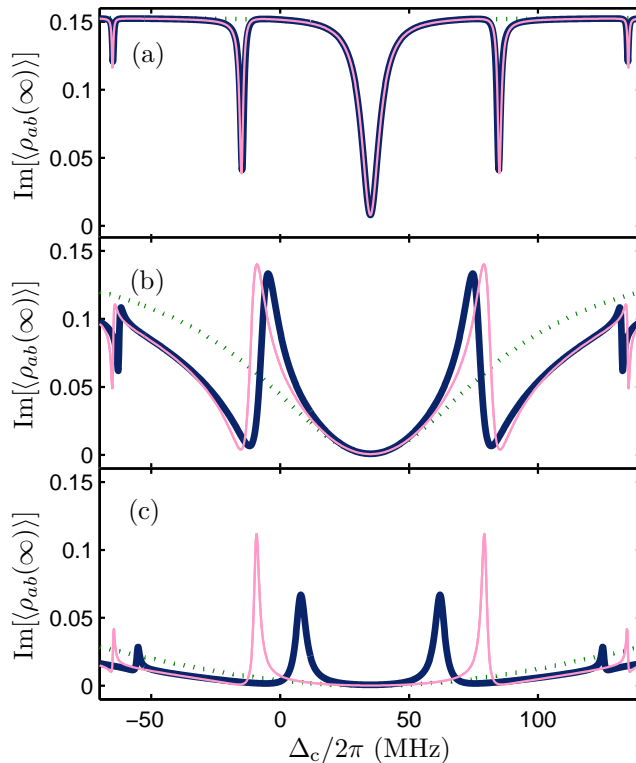


FIG. 7: (color online) Probe absorption vs. control laser detuning in an rf-dressed 3-level system, for three different control Rabi frequencies. The parameters of the system are the same as in Figs. 5 and 6, but here the probe field is on-resonance ( $\Delta_p = 0$ ) and  $\Delta_c$  varies.  $\Omega_c/2\pi$  is 8 MHz in (a), 30 MHz in (b) and 60 MHz in (c). Thick blue solid curves: results obtained by solving the full optical Bloch equations, Eqs. (43a–43f). Thin pink solid curves: results obtained in the  $N$ -level approximation, Eqs. (44a–44f). Dotted green curves: absorption profile without rf field (the energy of the Rydberg state was shifted by  $\Sigma_c$  to facilitate the comparison with the other results). As  $\Omega_c$  increases, the EIT transparency window in (a) expands into the sidebands region and the EIT absorption dips change into absorption peaks. The width of the features is modulated by the square of the Bessel function factors  $J_n$ .

occur at the detunings at which state  $|a\rangle$  is resonant with the dressed state formed by the states  $|b\rangle$  and  $|c\rangle$  coupled by the control field. The same changes are observed in the  $N$ -level approximation, at least for the parameters considered, but the position of the absorption features is more and more incorrect.

The green dotted curves represent the absorption profile calculated without the sidebands of state  $|c\rangle$  (but taking its Stark shift into account). Comparing these results to the thick

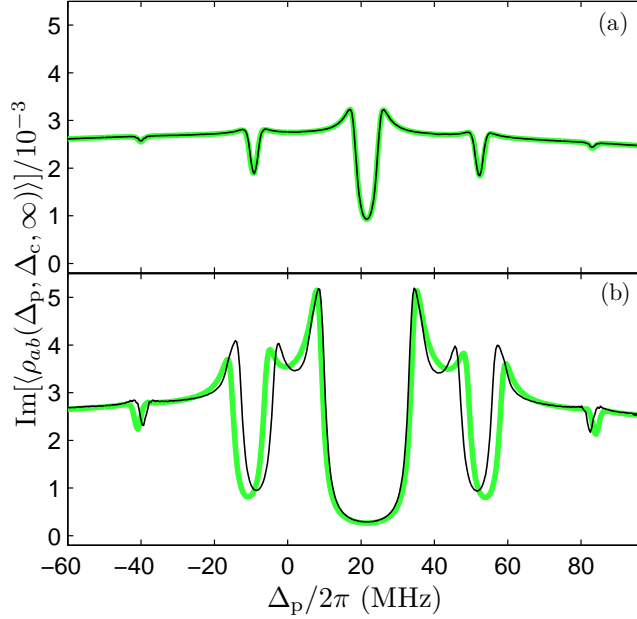


FIG. 8: (color online) The probe absorption in the same rf-dressed 3-level system as in Fig. 7 but here with Doppler averaging and plotted against probe detuning. The probe and control laser beams are assumed to be colinear and counterpropagating.  $\Omega_c/2\pi$  is 8 MHz in (a) and 30 MHz in (b).  $\Delta_c = 0$  in both graphs. Thick green curves: results obtained by solving the full optical Bloch equations, Eqs. (43a–43f). Thin black curves: results obtained in the  $N$ -level approximation, Eqs. (44a–44f). The higher power of the control field in (b) results in a broadening and a shift of the EIT dips and to inaccuracies in the  $N$ -level approximation.

blue curve in Fig. 7(c) shows that the suppression of EIT in narrow ranges of frequencies at large control powers arises from the interplay between these sidebands.

## 2. Thermal atomic ensembles

Let us assume that the two laser beams are colinear and counterpropagating. Compared to an atom at rest, the probe and control angular frequencies for an atom moving with a velocity component  $v$  in the direction of the control laser beam are shifted respectively by  $k_p v$  and  $-k_c v$ , where  $k_p$  and  $k_c$  are the wave numbers in the laboratory frame. In the reference frame of the atom, the probe detuning is therefore upshifted to  $\Delta_p + k_p v$  and the control detuning downshifted to  $\Delta_c - k_c v$ , where  $\Delta_p$  and  $\Delta_c$  are the detunings in the

laboratory frame. The absorption of the probe beam at  $\Delta_p$  and  $\Delta_c$  will thus be determined by the velocity average of the steady-state coherence  $\langle \rho_{ab}(\infty) \rangle$  calculated at the Doppler-shifted detunings. We denote this average by  $\langle \rho_{ij}(\Delta_p, \Delta_c, \infty) \rangle_{av}$ . For atoms of mass  $m$  at a temperature  $T$ ,

$$\langle \rho_{ij}(\Delta_p, \Delta_c, \infty) \rangle_{av} = \int_{-\infty}^{\infty} f(v) \langle \rho_{ij}(\Delta_p + k_p v, \Delta_c - k_c v, \infty) \rangle dv \quad (48)$$

with

$$f(v) = \sqrt{\frac{m}{2\pi k_B T}} \exp\left(-\frac{mv^2}{2k_B T}\right), \quad (49)$$

where  $k_B$  is the Boltzmann constant.

Fig. 8 shows the probe absorption calculated using the  $N$ -level approximation (thin black curves) or calculated directly from Eqs. (43a–43f) (thick green curves), as a function of the probe detuning, for two different values of  $\Omega_c$ . The other parameters are the same as those used in Fig. 5. In the Doppler average, we assume a cloud of  $^{85}\text{Rb}$  atoms at a temperature of 40 °C, and probe and control wavelengths of 780 and 480 nm, respectively.

We see that the  $N$ -level approximation is accurate in the case of figure (a), for which the control power is relatively low. For small values of  $\Omega_c$ , each absorption minimum corresponds to EIT in the velocity class which simultaneously satisfies the two conditions  $\Delta_p + k_p v = 0$  and  $\Delta_c - k_c v - \Sigma_c + 2n\omega_{rf} = 0$ . For a fixed value of  $\Delta_c$ , the corresponding absorption dips occur at the probe detunings

$$\Delta_p = \frac{k_p}{k_c}(\Sigma_c - \Delta_c - 2n\omega_{rf}). \quad (50)$$

Adjacent EIT dips are thus separated in probe detuning by  $2\omega_{rf} k_p/k_c$  in these conditions.

Increasing  $\Omega_c$  both widens the EIP dips through power broadening and shifts their positions. The latter effect is due to the shift in the sidebands of  $|c\rangle$  arising from their coupling with state  $|b\rangle$ . When this shift is non-negligible, the second of the above resonance conditions must be replaced by  $\Delta_c - k_c v - \Sigma_c + 2n\omega_{rf} - \delta_n = 0$ , where  $\delta_n$  is an  $\Omega_c$ -dependent shift, and the absorption dips occur at the probe detunings

$$\Delta_p = \frac{k_p}{k_c}(\Sigma_c - \Delta_c - 2n\omega_{rf} + \delta_n). \quad (51)$$

As seen from the figure, the  $N$ -level approximation becomes inaccurate when  $\Omega_c/(2\pi)$  is increased from 8 to 30 MHz: at the higher control power there is a clear difference both in the position and in the depth of the EIT dips between the absorption profiles calculated

with and without making this approximation. (Correcting the  $N$ -level approximation for the sidebands of the intermediate state, still neglecting the sidebands of the lower states, restores the agreement with the exact results.)

#### IV. SUMMARY

To conclude, we have investigated the absorption spectrum of two- and three-level model atomic systems with ac-modulated quadratic Stark shift, both in the weak coupling regime and beyond this regime. Although we specifically consider the case of a Rydberg system modulated by a radio-frequency field, our results are generic.

The different regimes investigated can be defined in terms of the modulation amplitude of the upper state energy, which is characterized by the quantity  $\Sigma_c$  defined by Eq. (7), and in terms of the angular frequency of the rf field,  $\omega_{\text{rf}}$ , of the Rabi frequency of the control field,  $\Omega_c$ , and of the natural width of the upper state,  $\Gamma_c$ . When the conditions  $|\Sigma_c| \ll 2\omega_{\text{rf}}$ ,  $|\Omega_c J_0(\Sigma_c/2\omega_{\text{rf}})| \ll 2\omega_{\text{rf}}$  and  $\Gamma_c \ll 2\omega_{\text{rf}}$  are all met, the quasienergy curve crossings in the Floquet spectrum (and the associated structures in the absorption spectrum) can be treated in isolation of each other. The system then behaves as if the most polarizable state is effectively a manifold of sideband states and the approximation we refer to as the  $N$ -level approximation is accurate. This approximation amounts to neglecting the manifold structure of the less polarizable states and model the ac modulated system as a many-level system in which these states interact with a manifold of independent sideband states spawned by the most polarizable state.

Increasing the strength of the control field to  $|\Omega_c J_0(\Sigma_c/2\omega_{\text{rf}})| \approx 2\omega_{\text{rf}}$  shifts the position of the absorption sidebands and changes their amplitude, in agreement with the perturbative analysis developed in a different context in Refs. [25] and [27] and with the iterative approach outlined in Sec. II B 2. The  $N$ -level approximation becomes inaccurate as  $|\Omega_c|$  increases, in particular in predicting sidebands shifts half too small. However, this approximation can be brought into agreement with the correct positions of the sidebands by a simple change in the optical Bloch equations (or the corresponding Hamiltonian).

In the strong coupling regime, where  $|\Omega_c J_0(\Sigma_c/2\omega_{\text{rf}})| \gg 2\omega_{\text{rf}}$ , the  $N$ -level approximation fails unless it is corrected by including the intermediate-state Floquet manifold in the model. For sufficiently large values of  $|\Omega_c|$ , the probe absorption spectrum in a 3-level ladder system

develops sidebands induced by the coupling of the intermediate state to the polarizable upper state, in addition to the sidebands manifesting in the weak coupling regime. For certain combinations of the parameters, this spectrum changes from one exhibiting sharp EIT dips to one exhibiting sharp absorption peaks as  $|\Omega_c|$  increases from  $|\Omega_c J_0(\Sigma_c/2\omega_{\text{rf}})| \ll 2\omega_{\text{rf}}$  to  $|\Omega_c J_0(\Sigma_c/2\omega_{\text{rf}})| \gg 2\omega_{\text{rf}}$ .

### Acknowledgments

We thank C. S. Adams for useful discussions at the early stages of this work and for his useful comments on the manuscript. We also thank the EPSRC and the DPST Programme of the Thai Government for financial support.

- 
- [1] M. Fleischhauer, M. Imamoglu, and J. P. Marangos, *Rev. Mod. Phys.* **77**, 633 (2005).
  - [2] M. Fleischhauer and M. D. Lukin, *Phys. Rev. Lett.* **84**, 5094 (2000)
  - [3] J. D. Pritchard, D. Maxwell, A. Gauguier, K. J. Weatherill, M. P. A. Jones, and C. S. Adams, *Phys. Rev. Lett.* **105**, 193603 (2010)
  - [4] A. V. Gorshkov, J. Otterbach, M. Fleischhauer, T. Pohl, and M. D. Lukin, *Phys. Rev. Lett.* **107**, 133602 (2011)
  - [5] D. Petrosyan, J. Otterbach, and M. Fleischhauer, *Phys. Rev. Lett.* **107**, 213601 (2011)
  - [6] M. Saffman, T. G. Walker, and K. Mølmer, *Rev. Mod. Phys.* **82**, 2313 (2010)
  - [7] J. D. Pritchard, C. S. Adams, and K. Mølmer, *Phys. Rev. Lett.* **108**, 043601 (2012)
  - [8] A. Osterwalder and F. Merkt, *Phys. Rev. Lett.* **82**, 1831 (1999)
  - [9] A. K. Mohapatra, M. G. Bason, B. Bustcher, K. J. Weatherill, and C. S. Adams, *Nature Phys.* **4**, 890 (2008)
  - [10] M. G. Bason, M. Tanasittikosol, A. Sargsyan, A. K. Mohapatra, D. Sarkisyan, R. M. Potvliege, and C. S. Adams, *New J. Phys.* **12**, 065015 (2010).
  - [11] D. Budker, D. F. Kimball, and D. P. DeMille, *Atomic Physics: An exploration through problems and solutions* (Oxford University Press, Oxford, 2004).
  - [12] D. I. Blochinzew, *Phys. Z. Sowjetunion* **4**, 501 (1933).
  - [13] C. H. Townes and F. R. Merritt, *Phys. Rev.* **72**, 1266 (1947).



- [14] S. H. Autler and C. H. Townes, *Phys. Rev.* **100**, 703 (1955).
- [15] J. E. Bayfield, L. D. Gardner, Y. Z. Gulkok, and S. D. Sharma, *Phys. Rev. A* **24**, 138 (1981).
- [16] H. B. van Linden van den Heuvell, R. Kachru, N. H. Tran, and T. F. Gallagher, *Phys. Rev. Lett.* **53**, 1901 (1984).
- [17] Y. Zhang, M. Ciocca, L.-W. He, C. E. Burkhardt, and J. J. Leventhal, *Phys. Rev. A* **50**, 1101 (1994).
- [18] T. Shirahama, X. M. Tong, K. I. Hino, and N. Toshima, *Phys. Rev. A* **80**, 043414 (2009).
- [19] C. S. E. van Ditzhuijzen, A. Tauschinsky, and H. B. van Linden van den Heuvell, *Phys. Rev. A* **80**, 063407 (2009).
- [20] D. Vion, A. Aassime, A. Cottet, P. Joyez, H. Pothier, C. Urbina, D. Esteve, and M. H. Devoret, *Science* **296**, 886 (2002).
- [21] Y. Yu, S. Han, X. Chu, Shih-I Chu, and Z. Wang, *Science* **296**, 889 (2002).
- [22] I. Chiorescu, Y. Nakamura, J. P. M. Harmans, and J. E. Mooij, *Science* **299**, 1869 (2003).
- [23] E. Collin, G. Ithier, A. Aassime, P. Joyez, D. Vion, and D. Esteve, *Phys. Rev. Lett.* **93**, 157005 (2004).
- [24] W. D. Oliver, Y. Yu, J. C. Lee, K. K. Berggren, L. S. Levitov, and T. P. Orlando, *Science* **310**, 1653 (2005).
- [25] S. K. Son, S. Han, and Shih-I Chu, *Phys. Rev. A* **79**, 032301 (2009).
- [26] J. Tuorila, M. Silveri, M. Sillanpää, E. Thuneberg, Y. Makhlin, and P. Hakonen, *Phys. Rev. Lett.* **105**, 257003 (2010).
- [27] J. Hausinger and M. Grifoni, *Phys. Rev. A* **81**, 022117 (2010).
- [28] These departures do not manifest in the results reported in Ref. [10]. However, measurements in the same ladder EIT system than in Ref. [10] but for higher Rydberg states and lower rf frequencies found sidebands separations differing from the usual  $2\hbar\omega_0$  spacing (M. Bason and C. S. Adams, unpublished).
- [29] J. H. Shirley, *Phys. Rev.* **138**, B979 (1965).
- [30] S. R. Barone and M. A. Narcowich, *Phys. Rev. A* **15**, 1109 (1977).
- [31] C. J. Joachain, N. J. Kylstra, and R. M. Potvliege, *Atoms in Intense Laser Fields* (Cambridge University Press, Cambridge, 2012).
- [32] Formally, and ignoring relaxation. the system formed by an atom exposed to both a laser field and an rf field can be described within the generalized multi-frequency Floquet theory

- [S.-I Chu, Adv. Chem. Phys. **73**, 739 (1989); M. Dörr, R. M. Potvliege, D. Proulx, and R. Shakeshaft, Phys. Rev. A **44**, 574 (1991)]. However, this general approach would be unnecessarily complicated here, since for the intensities and frequencies of interest the atom can be accurately represented as a two-level system with a periodic perturbation of the energy of one of the two states.
- [33] Rabi frequencies are assumed to be real, not complex, throughout the paper.
- [34] M. Pont, R. M. Potvliege, R. Shakeshaft, and Z.-J. Teng, Phys. Rev. A **45**, 8235 (1992).
- [35] The signs in Eqs. (13), (13) and (15) are chosen in such a way that the eigenstates of  $H'_{2F}$  belonging to the zero- $\Omega_c$  quasienergies  $\epsilon_{b,n}^{(0)}$  and  $\epsilon_{c,n}^{(0)}$  defined in Sec. II B 2 are, respectively,  $|b', n\rangle\rangle$  and  $|c', n\rangle\rangle$ , not  $|b', -n\rangle\rangle$  and  $|c', -n\rangle\rangle$ .
- [36] Eqs. (28a), (28b) and (34) are consistent with the results of Ref. [25].
- [37] Perturbation theory gives  $\tilde{\Delta}_{c,\pm m} \approx \Sigma_c \pm 2m\omega_{\text{rf}} \mp \tilde{\delta}_m^{\text{pt}}$  with  $\tilde{\delta}_m^{\text{pt}} = \sum_{m \neq -n} (\Omega_c J_m / 2)^2 / [2\omega_{\text{rf}}(m + n)]$ . Since  $\tilde{\delta}_m^{\text{pt}}$  is approximately half the correct shift, the  $N$ -level approximation can be improved by replacing  $\Sigma_c - \Delta_c \pm 2m\omega_{\text{rf}}$  by  $\Sigma_c - \Delta_c \pm 2m\omega_{\text{rf}} \mp \tilde{\delta}_m^{\text{pt}}$  in the diagonal elements of the matrix  $\tilde{H}'_{2F}$ , or equivalently by replacing  $\Sigma_c - \Delta_c - 2k\omega_{\text{rf}}$  by  $\Sigma_c - \Delta_c - 2k\omega_{\text{rf}} + \tilde{\delta}_k^{\text{pt}}$  in Eqs. (32a–32c).
- [38] P. M. Radmore and P. L. Knight, J. Phys. B: At. Mol. Phys. **15**, 561 (1982).
- [39] A. F. Linskens, I. Holleman, N. Dam, and J. Reuss, Phys. Rev. A **54**, 4854 (1996).
- [40] As discussed in Sec. II B 2, the sidebands do not occur exactly at  $\Sigma_c + 2n\omega_{\text{rf}}$ . However, for the parameters of Fig. 7(a), the difference is too small to be seen.
- [41] J. Gea-Banacloche, Y. Li, S. Jin, and M. Xiao, Phys. Rev. A **51**, 576 (1995).